REVIEW

National Science Review
8: nwab010, 2021
https://doi.org/10.1093/nsr/nwab010
Advance access publication 16 January 2021

MATERIALS SCIENCE

Selective catalytic reduction of NO_x with NH_3: opportunities and challenges of Cu-based small-pore zeolites

Yulong Shan[1], Jinpeng Du[1,3], Yan Zhang[2], Wenpo Shan[2], Xiaoyan Shi[1,3], Yunbo Yu[1,2,3], Runduo Zhang[4], Xiangju Meng[5], Feng-Shou Xiao[5] and Hong He[1,2,3,*]

[1]State Key Joint Laboratory of Environment Simulation and Pollution Control, Research Center for Eco-Environmental Sciences, Chinese Academy of Sciences, Beijing 100085, China; [2]Center for Excellence in Regional Atmospheric Environment, Institute of Urban Environment, Chinese Academy of Sciences, Xiamen 361021, China; [3]College of Resources and Environment, University of Chinese Academy of Sciences, Beijing 100049, China; [4]State Key Laboratory of Chemical Resource Engineering, Beijing Key Laboratory of Energy Environmental Catalysis, Beijing University of Chemical Technology, Beijing 100029, China and [5]Key Laboratory of Applied Chemistry of Zhejiang Province, Department of Chemistry, Zhejiang University, Hangzhou 310007, China

*Corresponding author. E-mail: honghe@rcees.ac.cn

Received 28 October 2020; **Revised** 28 December 2020; **Accepted** 11 January 2021

ABSTRACT

Zeolites, as efficient and stable catalysts, are widely used in the environmental catalysis field. Typically, Cu-SSZ-13 with small-pore structure shows excellent catalytic activity for selective catalytic reduction of NO_x with ammonia (NH_3-SCR) as well as high hydrothermal stability. This review summarizes major advances in Cu-SSZ-13 applied to the NH_3-SCR reaction, including the state of copper species, standard and fast SCR reaction mechanism, hydrothermal deactivation mechanism, poisoning resistance and synthetic methodology. The review gives a valuable summary of new insights into the matching between SCR catalyst design principles and the characteristics of Cu^{2+}-exchanged zeolitic catalysts, highlighting the significant opportunity presented by zeolite-based catalysts. Principles for designing zeolites with excellent NH_3-SCR performance and hydrothermal stability are proposed. On the basis of these principles, more hydrothermally stable Cu-AEI and Cu-LTA zeolites are elaborated as well as other alternative zeolites applied to NH_3-SCR. Finally, we call attention to the challenges facing Cu-based small-pore zeolites that still need to be addressed.

Keywords: environmental catalysis, Cu-SSZ-13, NH_3-SCR, reaction mechanism, small-pore zeolites

INTRODUCTION

General introduction to zeolite catalysts, NO_x pollution and SCR technology

Zeolites are a group of crystalline inorganic materials with regular pore structures that consist of connected TO_4 tetrahedra (T represents the framework atom) sharing oxygen atoms. Generally, the zeolites can be divided into small-pore zeolites with 8-membered rings (pore size of ∼4.0 Å), medium-pore zeolites with 10-membered rings (pore size of ∼5.5 Å), large-pore zeolites with 12-membered rings (pore size of ∼7.5 Å) and ultra-large-pore zeolites with >12-membered rings. The pore size of zeolites is similar to molecular sizes, which endows the zeolites with a molecular sieving effect, resulting in excellent shape selectivity. Their inner channel and cavity space give zeolites huge specific surface areas. Zeolite materials also have high hydrothermal stability due to their highly crystalline framework structure. Moreover, the abundant acid sites of zeolites can be easily adjusted by ion-exchange methods to satisfy the conditions of various chemical reactions. Based on these advantages, therefore, zeolites are widely used in the petrochemical, energy and environmental fields as efficient and stable catalysts [1–3]. An atomic-scale understanding of zeolite applications in different fields is of guiding significance to the design and synthesis of zeolite catalysts. The present work focuses on the field of environmental catalysis, in which zeolite catalysts play an indispensable role.

In the environmental field, nitrogen oxides (NO_x, including NO and NO_2) are important precursor pollutants for haze, photochemical smog and acid rain. In China, transportation contributes

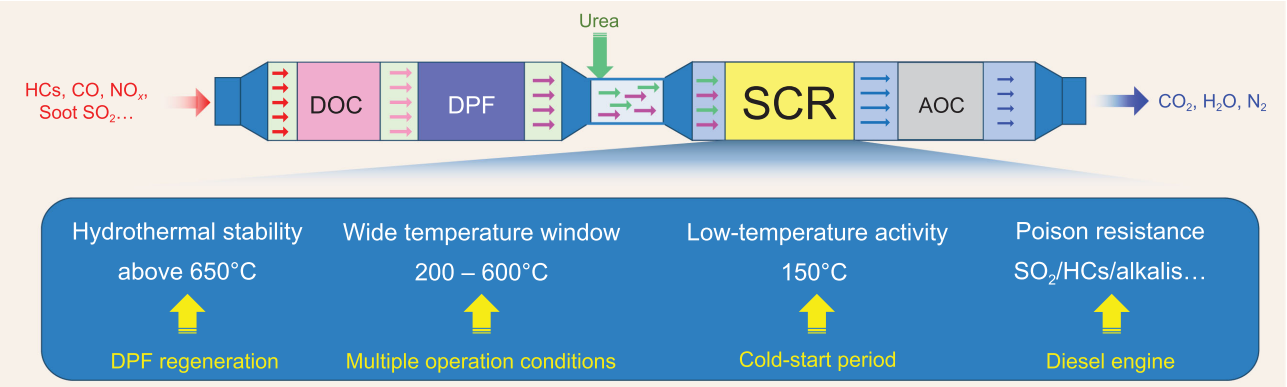

Figure 1. DOC + DPF + SCR + AOC aftertreatment system of diesel vehicles.

~35% of NO_x emissions, second only to industry (~40%) as an emissions source [4]. Diesel vehicles, which account for about 10% of automobiles, produce nearly 90% of NO_x (total ~6.4 million tonnes) emitted from automobiles [5]. In addition, non-road mobile sources, which primarily use diesel engines as a power source and include engineering machinery, farming machinery and marine engines, contributed comparable NO_x emissions to those of road automobiles in China. Therefore, controlling the NO_x pollutants emitted from diesel engines is urgent and imperative. The SuperTruck Program and Horizon 2020 were launched by the United States and the European Union to increase engine efficiency and reduce pollutants. China will also implement the China VI Standards for emissions from diesel-fuelled heavy-duty vehicles. In the aftertreatment system, the three-way catalyst (TWC) has difficulty controlling NO_x emissions due to the lean combustion conditions in diesel engines. For controlling diesel vehicle exhaust, the selective catalytic reduction of NO_x with ammonia (NH_3-SCR) has been successfully and commercially applied because of its high NO_x efficiency in the presence of excess oxygen.

To meet progressively more rigorous legislations and policies, a complicated aftertreatment system was proposed and employed comprising multiple processing units (Fig. 1), in which the SCR unit is located in a downstream position. The DOC (diesel oxidation catalyst) is used to oxidize the hydrocarbons (HCs) and CO and partially oxidize NO to NO_2 with excess oxygen. The partial oxidation of NO benefits the fast SCR reaction, which requires an equimolar mixture of NO and NO_2. PMs (particulate matters) are captured and filtered by the DPF (diesel particulate filter). The reason for the placement of the AOC (ammonia oxidation catalyst) is to eliminate NH_3 slip from the SCR unit. As can be seen, the SCR catalyst must have excellent hydrothermal stability due to the high-temperature environment (above 650°C) resulting from regeneration of the upstream DPF. Additionally, the complicated and changeable operation conditions of diesel vehicles expose the SCR catalyst to a wide variety of temperatures (200–600°C), including low temperatures below 200°C under cold-start and low-load conditions. Catalyst poisoning is also inevitable due to the incomplete oxidation of HCs and CO as well as the presence of S- and alkali-metal-containing diesel fuels. Therefore, SCR catalysts should be evaluated comprehensively and satisfy various operating modes in actual application. Fortunately, the zeolite catalysts are well-qualified as SCR catalysts due to their outstanding deNO_x efficiency, high hydrothermal stability and optimal poison resistance.

NH_3-SCR reaction features and NH_3-SCR catalysts

The NO_x emitted from diesel engines consists of 90% NO and 10% NO_2. Therefore, the primary reaction of NH_3-SCR is the standard SCR reaction (SSCR, reaction (1)). In this redox reaction, 12 electrons are transferred. The N (−3 valence) in NH_3 transfers $8e^-$ and $4e^-$ to NO and O_2, respectively. Oxygen participates in the oxidation of active sites and combines with hydrogen to form H_2O. Fast SCR (FSCR, reaction (2)), involving equal amounts of NO and NO_2, also occurs when NO is partially oxidized in the DOC unit. Through this reaction, higher NO_x conversion can usually be achieved, in which two and four electrons are transferred from NH_3 to NO and NO_2, respectively. Besides the standard and fast SCR reactions, there are also several side reactions (reactions (3–6)):

$$4NH_3 + 4NO + O_2 \rightarrow 4N_2 + 6H_2O \quad (1)$$

$$2NH_3 + NO + NO_2 \rightarrow 2N_2 + 3H_2O \quad (2)$$

$$6NO_2 + 8NH_3 \rightarrow 7N_2 + 12H_2O \quad (3)$$

$$4NH_3 + 3O_2 \rightarrow 2N_2 + 6H_2O \quad (4)$$

$$2NH_3 + 2O_2 \rightarrow N_2O + 3H_2O \quad (5)$$

$$4NH_3 + 4NO + 3O_2 \rightarrow 4N_2O + 6H_2O \quad (6)$$

The NH_3-SCR reaction needs the participation of both NO_x (acid oxide) and NH_3 (base). Therefore, dual-functional sites are of significant importance in the SCR reaction due to the double-cycle mechanism, including the redox cycle (NO_x) and acid cycle (NH_3). In addition, the tight coupling of redox and acid sites (redox-acid sites) is beneficial in taking advantage of the synergistic effects of dual-sites [6,7]. For example, Fe-Ti and Ce-W oxide catalysts were developed and showed excellent NH_3-SCR performance. The tight coupling of Fe (Ce) and Ti (W) is achieved by the co-precipitation method [7]. From another aspect, high dispersion and adequate exposure of functional sites, which increase the effective collision probabilities between active centres and reactants, are indispensable in every catalytic reaction.

Based on the above design principles, a series of redox-acid oxides with highly dispersed active sites were developed as novel and highly efficient NH_3-SCR catalysts [7,8]. However, the thermal stability of oxide catalysts still needs to be improved due to the phase separation of the tight coupling structure of redox and acid sites at high temperatures. Since the Cu-SSZ-13 small-pore zeolite was reported to have superior activity and hydrothermal stability in the NH_3-SCR reaction compared with medium- and large-pore zeolites (patent in 2009) [9–11], studies on Cu-SSZ-13 showed a dramatic increase in the past decade. The small-pore structure is primarily responsible for the high stability of the catalyst framework and active sites in Cu-SSZ-13 [11]. Concomitantly, other zeolites with similar small-pore structures, such as LTA, AEI, KFI, and RTH, also received much attention due to their comparable NH_3-SCR performance and/or hydrothermal stability to Cu-SSZ-13. In this work, the selective catalytic reduction of NO_x using the Cu-SSZ-13 zeolite catalyst is comprehensively reviewed with critical emphasis on the state of active sites, SCR reaction mechanism and synthetic methods, as well as poisoning resistance mechanisms (SO_2, PO_4^{3-}, HCs, alkali and alkaline earth metals). Based on the research methodology employed for Cu-SSZ-13, other Cu-exchanged small-pore zeolites are described in detail. Great efforts have been made to achieve matching between the characteristics of Cu^{2+}-exchanged small-pore zeolite and highly efficient NH_3-SCR catalysts, which is of great importance for the design of high-efficiency zeolitic catalysts. Furthermore, we propose basic rules for designing a zeolite catalyst for the NH_3-SCR reaction as well as future efforts in this research field. We are devoted to providing an easy-to-read and systematic review of SCR of NO_x using Cu^{2+}-exchanged small-pore zeolites as catalysts and to highlighting the opportunities and challenges of Cu-based small-pore zeolites.

Cu-SSZ-13: A MODEL CASE FOR Cu^{2+}-EXCHANGED ZEOLITE CATALYSTS FOR NH_3-SCR

As we discussed above, the highly efficient NH_3-SCR catalysts contain tightly coupled redox-acid sites as well as high dispersion and adequate exposure of these functional sites. Remarkably, the characteristics of copper ion-exchanged zeolites match perfectly with NH_3-SCR catalyst requirements, as shown in Fig. 2. The Cu^{2+}/Cu^{+} couple can act as

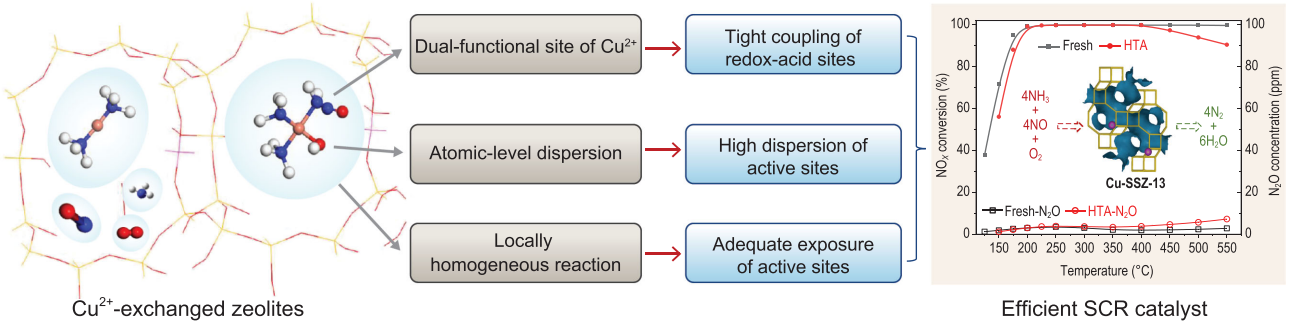

Figure 2. Matching between the characteristics of Cu^{2+}-exchanged zeolitic catalyst and SCR catalyst requirements. The monolithic catalyst (~2.36 cm^3) was estimated to have a total gas flow of 1.67 L/min, resulting in GHSV of ~42 000 h^{-1}. HTA represents that the sample was hydrothermally aged at 750°C for 16 h.

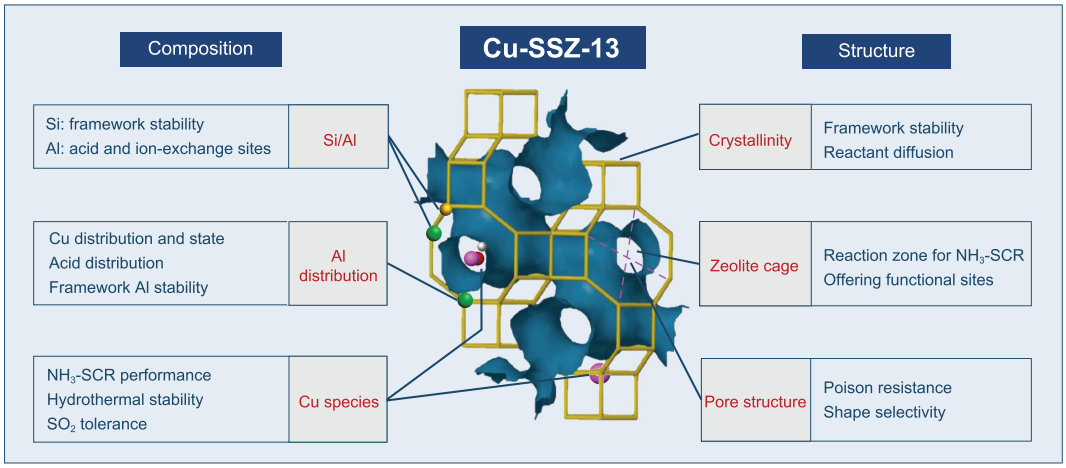

Figure 3. The composition-structure-activity (stability) relationship of Cu-zeolites for NH_3-SCR reaction.

both redox and acid site in the NH_3-SCR reaction due to its multi-valence state and Lewis acid characteristics, where the redox cycle (NO_x) and acid cycle can both be completed; moreover, the Cu^{2+} ions in ion-exchanged zeolites are atomically dispersed, since the metal ions compensate the positive charge of the zeolite framework by anchoring on the ion-exchange sites. More importantly, the locally homogeneous reactions in the bulk phase, resulting from the dynamic NH_3-solvated Cu ions and electronic effects of the zeolite, significantly increase the effective collision probability between reactants and active species [12]. Therefore, Cu^{2+}-exchanged zeolites achieve the required attributes of tight coupling of redox-acid sites, high dispersion and adequate exposure of functional sites. In particular, small-pore zeolites such as Cu-SSZ-13 possess better NH_3-SCR performance and higher hydrothermal stability, N_2 selectivity and poisoning tolerance than other zeolites due to the peculiar small-pore structure. For example, the small pores (~4.0 Å) of Cu-based small-pore zeolites inhibit dealumination of the framework and accumulation of copper species during hydrothermal aging, which is highly beneficial for hydrothermal stability [11]. Also, some poisons, such as long-chain hydrocarbons, are prevented from entering the small pores due to their shape selectivity. The cavities of small-pore zeolites offer abundant active sites and large reaction zones, thus facilitating the chemical reactions. Therefore, the NH_3-SCR reaction requirements match perfectly with the physicochemical properties of Cu^{2+}-exchanged zeolites (especially small-pore zeolites), providing a solid foundation for highly efficient and stable NH_3-SCR zeolite catalysts.

Due to the excellent deNO_x efficiency and hydrothermal stability as well as the simplicity of the framework structure (only one T site), Cu-SSZ-13 zeolite, with chabazite (CHA) topology, is studied as a model case for understanding the composition-structure-activity (and stability) relationship of Cu^{2+}-exchanged zeolite catalysts applied for NH_3-SCR. As shown in Fig. 3, the CHA structure is constructed by stacking double six-membered rings (D6R) in an ABC sequence, resulting in a large CHA cavity and eight-membered ring (8MR) pore structure. The Si/Al ratio is of vital importance for the performance of Cu-SSZ-13 zeolite as an SCR catalyst. The large amount of Si in the substrate assures the stability of the zeolite framework, and the substitution of Si by Al provides acid sites due to charge compensation, which further benefits the location of active metal ions during the ion-exchange process and NH_3 adsorption during the NH_3-SCR reaction. Consequently, the Cu and acid site distribution as well as its stability are determined by the Al distribution in Cu-SSZ-13 zeolites. The state and location of Cu species directly affect the NH_3-SCR performance, hydrothermal stability and SO_2 tolerance of Cu-exchanged zeolites. As for the zeolite structure, the high crystallinity of zeolite favours framework stability and reactant diffusion. Reaction zones for NH_3-SCR and adequate functional sites can be offered by the large zeolite cage (such as the CHA cavity). Importantly, the pore structure endows Cu-exchanged zeolites with shape selectivity catalysis, leading to high poison resistance, especially regarding some large molecules. After describing the general characteristics of Cu-SSZ-13, the application of Cu-SSZ-13 in the NH_3-SCR reaction is elaborated in detail below.

Copper species

The state and location of copper species are closely related to the elemental composition of the zeolite

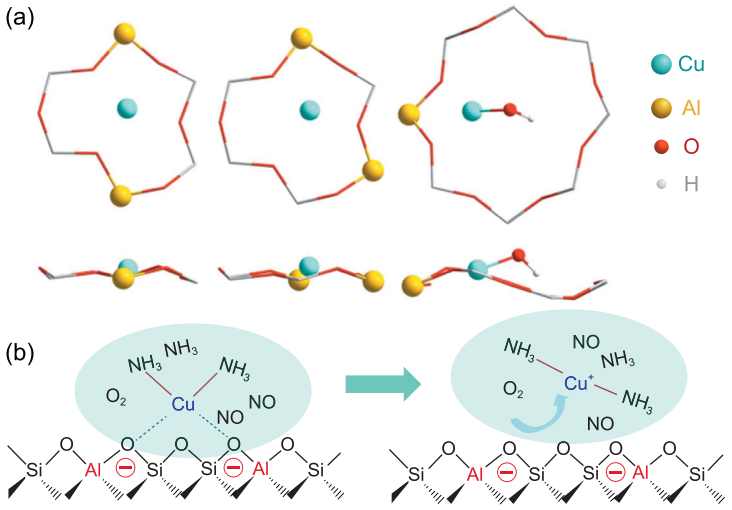

Figure 4. (a) Density functional theory (DFT) calculations of Cu^{2+} location and coordination. Adapted with permission from ref. [16]. (b) The NH_3 solvation effect of Cu^{2+} and dynamic Cu-$(NH_3)_n$ complex during SCR reaction.

and the atmospheric environment. The substitution of Si atoms by Al atoms creates charge defects, which provide Brønsted acid sites and exchange sites for Cu ions. The isolated Cu^{2+} ions were initially thought to be the active centres and to be coordinated to three oxygen atoms of the six-membered rings (6MRs) [13,14]. However, Kwak *et al.* identified two types of Cu ions at distinct cationic positions in Cu-SSZ-13 zeolite when Cu/Al is higher than 0.2 via H_2-TPR and fourier transform infrared (FTIR) measurements [15]. Afterwards, researchers depicted the location and coordination of the two types of Cu ions (Fig. 4a) [16,17]. The relatively stable Cu^{2+} ions, which compensate paired negative charge (labelled as Cu^{2+}-2Al), are located in the windows of 6MRs. After saturation of paired Al, $[CuOH]^+$ ions appear subsequently and populate single framework Al sites next to 8MRs (labelled as $[Cu(OH)]^+$-Al). Consequently, the amount of active copper species can be adjusted by tuning the Al contents and distribution. For example, with the increase of Al content (from Si-rich zeolites to Al-rich zeolites), the capacity for Cu^{2+}-2Al species increases due to the presence of large amounts of paired Al, and the $[Cu(OH)]^+$-Al species appear only at high Cu/Al [17]. The Al distribution at a fixed Si/Al ratio can be adjusted by using different structure-directing agents (SDAs) to synthesize the SSZ-13 substrate. Iorio *et al.* found that the density of paired Al increased linearly with the Na^+ content incorporated into the crystallized solid when using $TMAda^+$ and Na^+ as organic and inorganic SDA [18,19]. Zhang *et al.* also increased the amounts of close Al sites in SSZ-13 by adjusting the crystallization pathways using $DMCHA^+$ as the organic template, generating more Cu^{2+}-2Al species than found in Cu-SSZ-13 synthesized using $TMAda^+$ as the organic template [20].

The atmospheric environment can also influence the Cu state and coordination, and is closely related to the low-temperature catalytic activity of active copper species in Cu-SSZ-13 zeolite. Generally, the copper species are in the hydrated state in the ambient air, represented as $[Cu(OH)(H_2O)_5]^+$ and $[Cu(H_2O)_6]^{2+}$ [17,21]. The coordination between Cu ions and the zeolite structure can be weakened by the solvation effect of H_2O. When increasing the temperature to ~250°C, the hydrated copper species will release bound water and become bound at the ion-exchange sites in the form of $[Cu(OH)]^+$-Al and Cu^{2+}-2Al [21]. Similarly, the copper species are solvated by ammonia much more strongly than by H_2O in the presence of NH_3. The formed Cu-NH_3 complex is thought to be the active site in the low-temperature NH_3-SCR reaction [12,22–24]. More importantly, the active sites are movable within a limited region (~9 Å) due to the weak bonding between Cu ions and the zeolite structure due to NH_3 solvation (Fig. 4b), which further increases the effective collision possibility between active sites and reactants in a local area. Meanwhile, concomitant with the solvation of copper species by NH_3, the reduction of Cu^{2+} ions takes place, resulting in NH_3-solvated Cu^+ ions [17,23]. Compared to Cu^{2+}-2Al, $[Cu(OH)]^+$-Al is more readily reducible by NH_3 to form $Cu(NH_3)_n^+$ and H_2O [17]. The mobile NH_3-solvated Cu^+ species, which play a pivotal role in the NH_3-SCR reaction, can also be generated in the actual NH_3-SCR atmosphere. Researchers have also found the 'auto-reduction' of Cu^{2+} ions in a vacuum, inert atmosphere and even O_2 atmosphere at high temperatures [21,25].

Standard SCR reaction mechanism

Great efforts have been devoted to uncovering the standard SCR (SSCR) reaction cycle of Cu-SSZ-13, including the reduction ($Cu^{2+} \rightarrow Cu^+$) and oxidation ($Cu^+ \rightarrow Cu^{2+}$) half-cycles. A seagull NO_x profile (Fig. 5a) with dual-maxima NO_x conversion was observed during the SSCR reaction over Cu-SSZ-13 catalysts with low Cu loading [22,26]. Figure 5b and c depict the linear relationship of the SSCR rate as a function of $(\text{Cu loading})^2$ and (Cu loading) at low and high temperatures, respectively [27]. Both of these indicate two distinct reaction regimes that require participation of paired Cu ions and isolated Cu ions at low and high temperatures, respectively.

A representative SSCR reaction cycle over Cu-SSZ-13 at low temperatures is shown in Fig. 5e. In the reduction half-cycle of SCR, Cu species

which act as both redox and Lewis acid sites are readily reduced under the coexistence of NH_3 and NO at low temperatures (below 250°C), leading to the formation of NH_3-solvated Cu^+ species, as discussed above [23,28,29]. In the oxidation half-cycle of SCR, binuclear Cu ions, which are achieved via the migration of $Cu(NH_3)_2^+$, are essential for O_2 activation based on the linear relationship between the standard SCR rate and (Cu loading)^2 [22]. The electrostatic tethering between $Cu(NH_3)_2^+$ and the zeolite structure becomes weak after NH_3 coordination, resulting in dynamic multinuclear active sites in a limited volume (Fig. 5d). Paolucci *et al.* calculated that the diffusion radius of $Cu(NH_3)_2^+$ is ∼9 Å, meaning that $Cu(NH_3)_2^+$ can travel through 8MR CHA windows to form binuclear Cu ions [12]. This mechanism is a breakthrough in catalytic chemistry because it is outside the scope of traditional heterogeneous and homogeneous reactions, behaving more like a locally homogeneous reaction (Fig. 5e). The density functional theory (DFT) calculation result reveals that O_2 activation (that is, formation of $Cu(NH_3)_2$-O_2-$Cu(NH_3)_2$) is the rate-determining step for the NH_3-SCR reaction over Cu-SSZ-13 [12,22,30]. Recently, Negri *et al.* identified the formation of a side-on μ-η^2, η^2-peroxo diamino dicopper (II) complex $[Cu_2(NH_3)_4O_2]^{2+}$ (Fig. 5f) during the reaction of linear $Cu(NH_3)_2^+$ with O_2 via wavelet transform analysis of the extended X-ray absorption fine structure (EXAFS) data with other auxiliary measurements [31]. Four electrons are required to complete the O_2 activation and dissociation. Therefore, NO was proposed to act as another electron provider in addition to two $[Cu(NH_3)]^+$, which can only deliver two electrons [22]. Using DFT calculations, Chen *et al.* investigated the reactivity of $[Cu_2(NH_3)_4O_2]^{2+}$ with NO by proposing two cycles, in which NO is adsorbed on Cu(II) sites to form NO^+ or oxygen to form NO_2^-. In their calculations, Brønsted acid sites play a pivotal role in the decomposition of HONO and H_2NNO intermediates formed on Cu sites, and the catalytic cycle is probably controlled by the orientation of HONO and H_2NNO from Cu sites to Brønsted acid sites [32]. By combining X-ray absorption spectroscopy (XAS) and ultraviolet-visible-near-infrared (UV-Vis-NIR) spectroscopies, Negri *et al.* found that NO + NH_3 and NO can react with the $[Cu_2(NH_3)_4O_2]^{2+}$ complexes, and an excess of the reactants leads to complete reduction of $[Cu_2(NH_3)_4O_2]^{2+}$ to linear $[Cu(NH_3)]^+$ accompanied by the formation of N_2, indicating the reaction of $[Cu_2(NH_3)_4O_2]^{2+}$ with NO [31].

Turning to the reaction mechanism at elevated temperatures (>300°C), isolated Cu ions anchor on the ion-exchange sites and become fixed in the zeolite framework due to the decomposition of $Cu(NH_3)n$ species, according to NH_3-TPD results [33]. The SSCR reaction activation energy at high temperatures (∼140 kJ/mol) is significantly higher than that at low temperatures (∼70 kJ/mol), indicating the presence of a different reaction pathway [27]. Janssens *et al.* proposed a reaction mechanism for the SSCR reaction based on isolated Cu^{2+}/Cu^+ ions [34], which is more like the reaction cycle at high temperatures (Fig. 5g). The Cu^{2+} ions are reduced by NO + NH_3 and re-oxidized by NO + O_2 or NO_2. They indicated that the oxidation of an NO molecule by O_2 to a form bidentate nitrate ligand is rate-determining for the SSCR.

Generally, most studies discuss the SSCR reaction cycle over the fresh Cu-SSZ-13 with low Cu loading, which simplifies the catalytic system with only a single Cu site. However, in actual application, the Cu loading of Cu-SSZ-13 is usually higher than the theoretical one. The NO reduction at high temperatures would decrease with the increase of Cu loading due to the occurrence of non-selective NH_3 oxidation by oxygen at high temperatures, which leads to a lack of reductant. Moreover, some Cu species in the deep pores cannot gain access to the reactants. Therefore, controlling the amount of active Cu sites is important for actual application of Cu-SSZ-13. In another aspect, when Cu-SSZ-13 is aged, the behaviour is much more complicated due to the presence of various Cu species (such as CuO_x). As a result, there have been few studies focusing on aged or high Cu-loaded Cu-SSZ-13. However, more studies should be conducted to understand the reaction process of aged or high Cu-loaded Cu-SSZ-13 zeolites, since these catalysts are closer to the actual situation in practice.

FSCR reaction and NH_4NO_3 formation

The FSCR reaction (reaction (2)) also plays an important role in NO_x reduction due to the presence of ∼10% NO_2 in actual diesel exhaust, as well as the partial oxidation of NO to NO_2 in the DOC section. Normally, NO_2 addition to the feed is an effective way of achieving high deNO_x efficiency for NH_3-SCR catalysts. Differently to most NH_3-SCR catalysts, however, Cu-SSZ-13 catalysts only showed a slight improvement in NO_x reduction under FSCR conditions, as reported by Kwak *et al.* [35]. Our group even found an inhibition effect on NO_x conversion over our *in situ* synthesized Al-rich Cu-SSZ-13 catalyst due to the formation of ammonium nitrate (Fig. 6a) [36,37]. Therefore, the small-pore zeolites scarcely rely on NO oxidation to achieve the FSCR reaction, unlike other SCR catalysts. The

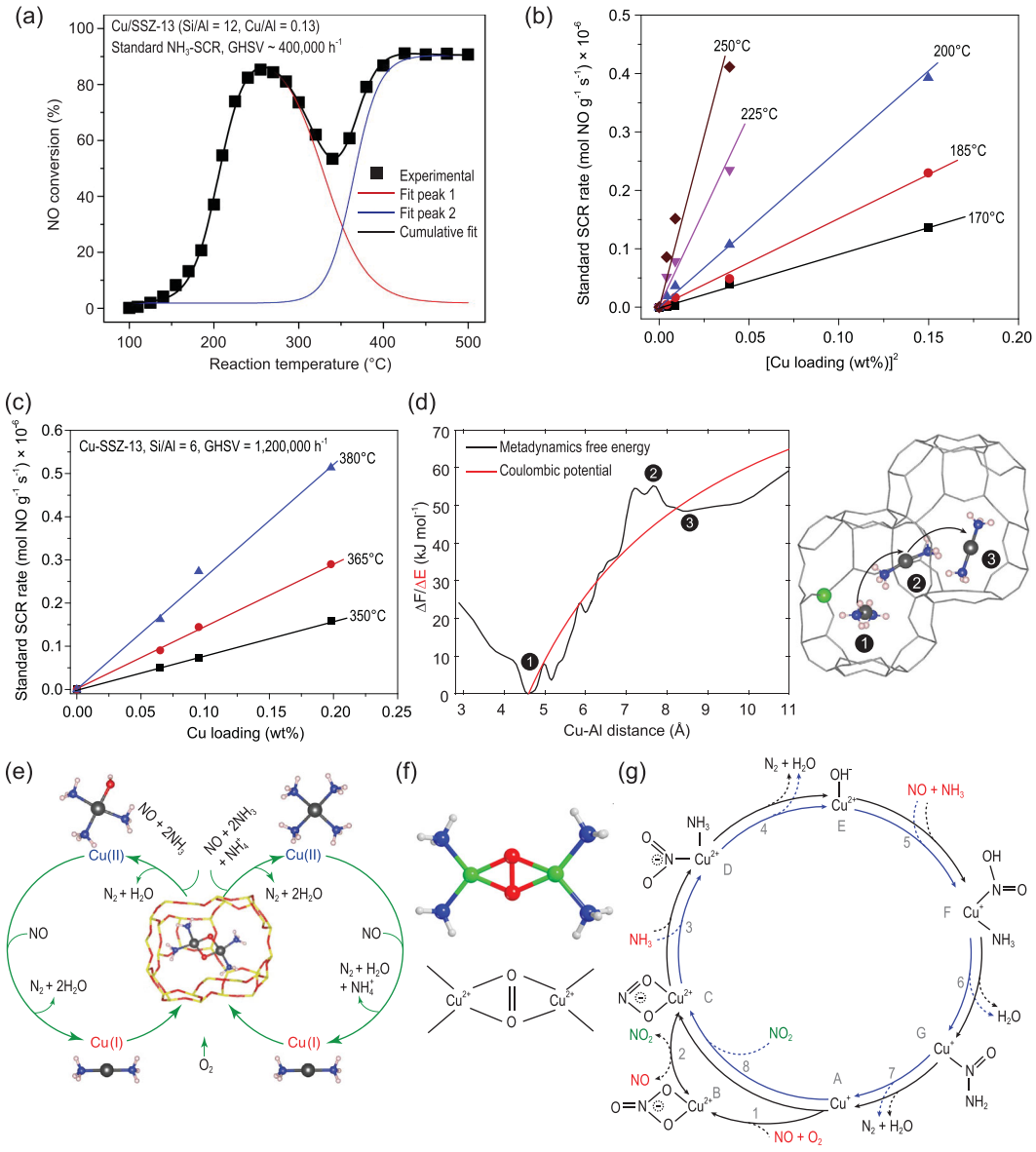

Figure 5. (a) NO conversion as a function of temperature over Cu-SSZ-13. Adapted with permission from ref. [22]. SCR rate over Cu-SSZ-13 as a function of (b) (Cu loading)^2 at low temperatures and (c) (Cu loading) at high temperatures. Adapted with permission from ref. [27]. (d) Free energy and diffusion of $Cu^{I}(NH_3)_2$ at different sites. Adapted with permission from ref. [12]. (e) Proposed low-temperature standard SCR catalytic cycle. Adapted with permission from ref. [12]. (f) Side-on μ-η^2, η^2-peroxo diamino dicopper (II) complex $[Cu_2(NH_3)_4O_2]^{2+}$ species. Adapted with permission from ref. [31]. (g) Possible high-temperature SCR catalytic cycle. Adapted with permission from ref. [34].

formation of surface NH_4NO_3 from the adsorbed NO_2 and NH_3 is a common reaction in the FSCR according to reaction (7), and NH_4NO_3 decomposition primarily takes place in two ways as shown in reaction (8) and reaction (9):

$$2NO_2 + 2NH_3 \rightarrow N_2 + NH_4NO_3 + H_2O \quad (7)$$

$$NH_4NO_3 \rightarrow N_2O + 2H_2O \quad (8)$$

$$NH_4NO_3 + NO \rightarrow NO_2 + N_2 + 2H_2O \quad (9)$$

The comparable geometric dimensions of the small pores (~3.8 Å) and reactant molecules (Fig. 6b) are mainly responsible for the strong inhibition of NO conversion activity, since a slight amount of NH_4NO_3 accumulation can limit the diffusion of reactants as well as $[Cu(NH_3)_2]^+$ species. Moreover, the NH_4NO_3 formed in small-pore zeolites is more stable than that in large-pore zeolites [38]. Our group investigated the effect of NO_2 on the NH_3-SCR reaction over Cu-SSZ-13 with varying Cu loadings [37]. We found that increased

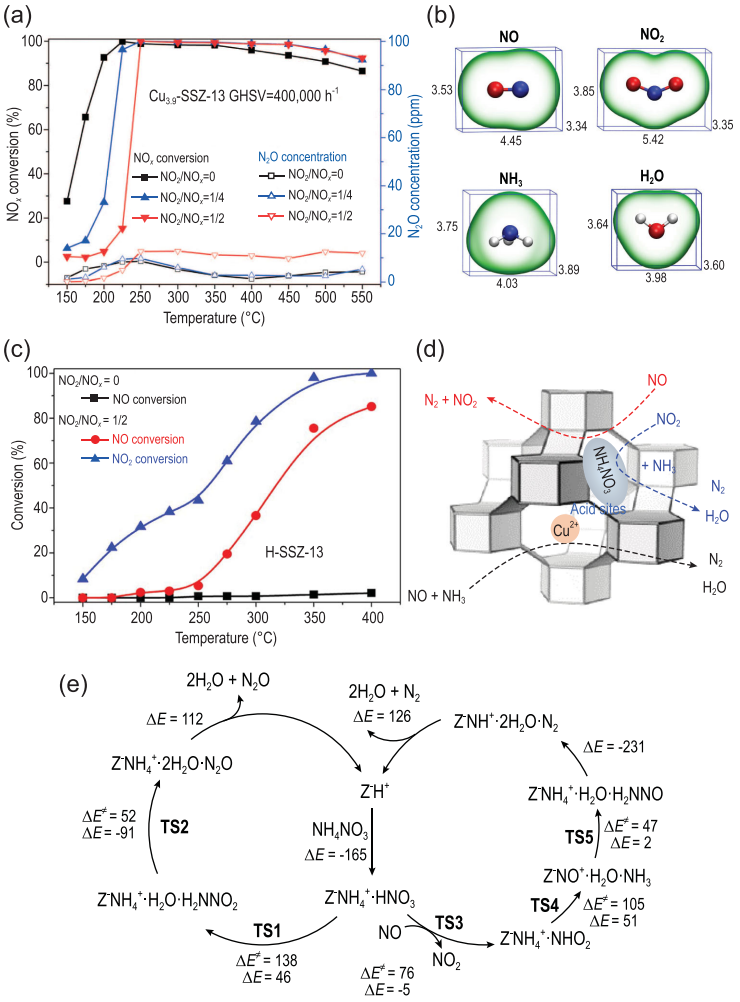

Figure 6. (a) NH_3-SCR performance of Cu-SSZ-13 under different reaction conditions. Adapted with permission from ref. [36]. (b) Different reaction pathways of NO and NO_2 over Cu-SSZ-13. Adapted with permission from ref. [37]. (c) NO, NO_2 and NO_x conversion on H-SSZ-13 under fast SCR conditions. Adapted with permission from ref. [37]. (d) Molecular size of NH_3, NO and NO_2. Adapted with permission from ref. [37]. (e) DFT-calculated reaction pathways for direct and NO-assisted NH_4NO_3 decomposition. Adapted with permission from ref. [39].

Cu loadings contributed to the SSCR reaction, while inhibiting the FSCR reaction. At low temperatures, the NO conversion activity was totally suppressed because of the formation of NH_4NO_3, while NO_2 could react with NH_3 at acid sites to contribute to NO_x conversion (Fig. 6d). Further, it was observed that the deposited NH_4NO_3 reacted with NO over H-SSZ-13 at high temperatures (Fig. 6c), accompanied by the direct decomposition of NH_4NO_3 to N_2O (reaction (8)). However, the N_2O production is less than 25 ppm. As shown in Fig. 6e, the DFT-calculated reaction pathways demonstrated that the energy barrier (105 kJ/mol) for NO-assisted NH_4NO_3 decomposition (reaction (9)) is much lower compared to that (138 kJ/mol) of direct NH_4NO_3 decomposition (reaction (8)) [39]. The combination of reaction (9) and reaction (7) yields the FSCR reaction (2), indicating that the FSCR reaction occurs only on Brønsted acid sites, which is also testified to by computational methods [39,40]. To avoid this inhibition phenomenon, we conducted hydrothermal aging to decrease the density of Brønsted acid sites to alleviate NH_4NO_3 accumulation and cause mesopore formation to favour gas diffusion [41]. As expected, the inhibiting effect of NO_2 on NO_x conversion was weakened for the hydrothermally aged Cu-SSZ-13 catalysts. In another aspect, what should be noted is that NH_4NO_3 accumulated only under steady-state conditions. Bendrich *et al.* found that almost no NH_4NO_3 is predicted to form during temperature oscillation and NO/NO_2 ratio oscillation [42,43]. The decomposition temperature of NH_4NO_3 formed on Cu-SSZ-13 is about ~225°C, which is easily exceeded during the driving cycle [37]. As for oscillating NO/NO_2 ratios, NH_4NO_3 can act as an NO_2 buffer that stores NO_2 under NO_2-excess conditions and decomposes under NO_2-deficient conditions.

There is a common consensus that NH_4NO_3 forms on Cu-SSZ-13 and inhibits NO_x conversion under FSCR conditions at steady-state and low temperatures. An atomic-level picture of the FSCR reaction cycle is still lacking, especially regarding the Cu sites. Research studies have only found Cu(II) species, due to the strong oxidizing ability of NO_2, and $Cu(NH_3)n$ complexes have scarcely been identified under FSCR conditions, making it difficult to investigate the reduction and oxidation half-cycle of the SCR reaction [12,44]. Moreover, the NH_4NO_3 formation and high reactivity of the SSZ-13 substrate limit the investigation of Cu active sites. The reaction cycle containing NO_2 shown in Fig. 5g is a rational candidate due to the presence of Cu(II) species coordinated strongly to zeolite and the absence of the $Cu(NH_3)_n$ complex. However, the evidence is not conclusive, and more studies are required in future.

Hydrothermal stability

For the aftertreatment system of diesel engines, excellent hydrothermal stability (HTS) is an indispensable property due to the high-temperature environment (above 650°C) resulting from regeneration of the upstream DPF. Cu-SSZ-13 small-pore zeolites were reported to have superior HTS to that of medium- and large-pore zeolites as well as most of the oxide catalysts [11]. Researchers have devoted much effort to unravelling

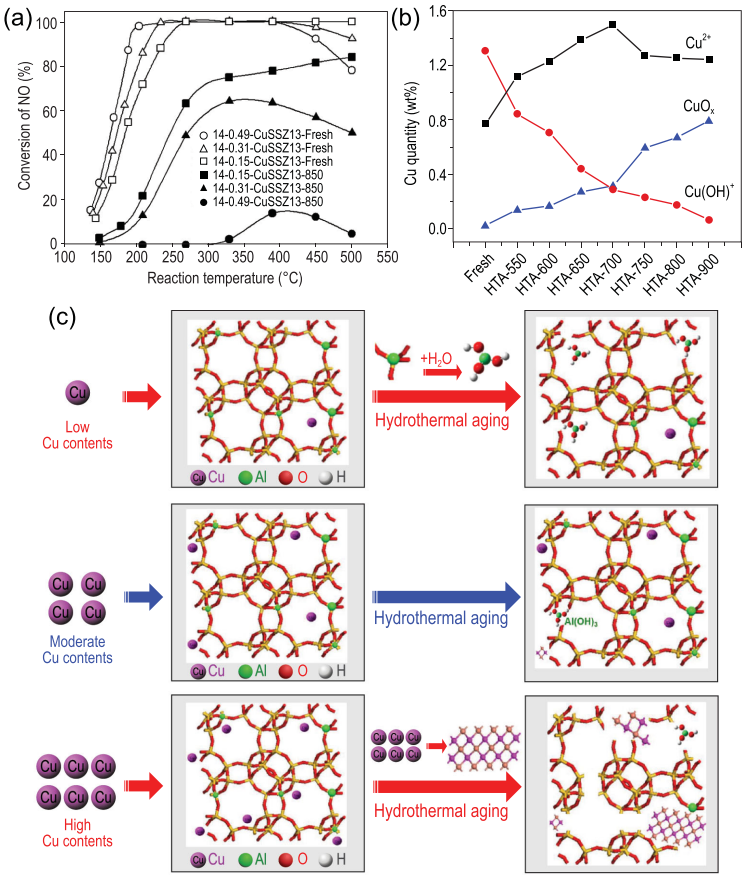

Figure 7. (a) Standard NH_3-SCR performance of fresh and HTA Cu-SSZ-13 with different Cu/Al ratios. Adapted with permission from ref. [46]. (b) Estimation of Cu^{2+}-2Al, $[Cu(OH)]^+$-Al and CuO_x in fresh and HTA samples. Adapted with permission from ref. [48]. (c) The deactivation mechanism of HTA of Cu-SSZ-13 with different Cu contents. Adapted with permission from ref. [51].

the deactivation mechanism of hydrothermal aging (HTA).

Hydrolysis of framework Al and accumulation of CuO_x from Cu^{2+} active sites are the two key reasons for HTA deactivation. The narrow small pores (~3.8 Å) block the diffusion of hydrolysed $Al(OH)_3$, with large kinetic diameter of ~5.03 Å, leading to its reattachment back into the structural defects caused by dealumination when the zeolite cools down [45]. This is the principal reason that small-pore zeolites have higher skeleton stability than medium- and large-pore zeolites during HTA. Regarding the effect of copper species, researchers found that HTS decreased with increasing Cu/Al ratio (Fig. 7a) [45–47]. As mentioned in 'Copper species' section, Cu^{2+}-2Al species with higher stability primarily exist in Cu-SSZ-13 catalysts with low Cu loading. Increasing Cu loading leads to formation of $[Cu(OH)]^+$-Al species, which easily accumulate to form CuO_x. This was also proved by Gao and co-workers using electron paramagnetic resonance (EPR) as the primary measurement [48,49]. They found that mild HTA first induced some conversion of $[Cu(OH)]^+$-Al to Cu^{2+}-2Al species, resulting in paired Cu^{2+} located in a D6R prism with a distance of ~3.90 Å [49]. Further increasing the HTA temperature, $[Cu(OH)]^+$-Al species gradually accumulated to form CuO_x clusters (Fig. 7b) [48].

The Si/Al ratio can also influence the HTS of Cu-SSZ-13 by affecting the copper distribution. Al-rich zeolites favour the presence of Cu^{2+}-2Al species, thus leading to higher HTS compared to Si-rich zeolites [46,50]. Nevertheless, the Al-rich zeolites still face the problem of dealumination, which will cause the loss of Brønsted acid sites during HTA, due to the large amount of vulnerable framework Al. We investigated the HTS of Al-rich Cu-SSZ-13 zeolite and found that Cu^{2+} ions inhibit dealumination of the SSZ-13 zeolite structure, while excessive quantities of them easily accumulate to form CuO_x clusters, leading to collapse of long-range order (Fig. 7c) [51]. Ye *et al.* also reported that preservation of active Cu^{2+} sites is more important than preserving Brønsted acid sites [52]. This is understandable, because Brønsted acid sites only serve as an NH_3 reservoir or probably as active sites for the decomposition of HONO and H_2NNO intermediates, as discussed in 'Standard SCR reaction mechanism' section, while the Cu^{2+} species can act as both redox and acid sites and can complete the NH_3-SCR reaction cycle on their own. Besides CuO_x, $CuAlO_x$ species were also detected by researchers [53–55]. Ma *et al.* found that $CuAlO_x$ originating from the combination of Cu with extra-framework Al is inert, while CuO_x species still have catalytic oxidation ability [55]. Schmidt *et al.* found evidence that Cu-SSZ-13 only shows Cu and Al clustering separately, while Cu-ZSM-5 contains large amounts of copper aluminate species after HTA, by using atom probe tomography technology, which can show the 3D distributions of component elements [54].

In summary, CuO_x formation and dealumination are two reasons for HTA deactivation, and interact during HTA. CuO_x accumulation can induce zeolite structure collapse, and extra-framework Al can coordinate with Cu to form $CuAlO_x$ species that are inert. As both redox and acid sites, Cu species are of vital importance and should be carefully tuned and protected. As an alternative, utilizing an Al-rich zeolite support is a simple and effective way to increase the HTS of Cu-SSZ-13 since the capacity for stable Cu^{2+}-2Al species is large due to the presence of many paired Al atoms in Al-rich zeolites.

Sulphur poisoning and desulphurization

Sulphur poisoning is an inevitable challenge due to the residual sulphur in diesel fuel. Figure 8a shows the SSCR performance of fresh, sulphated and

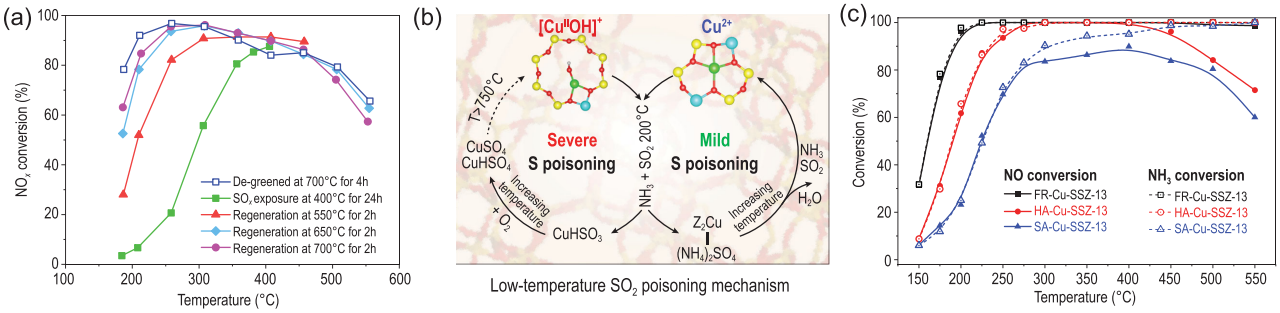

Figure 8. (a) Effect of SO_x exposure and subsequent thermal deSO_x. Adapted with permission from ref. [56]. (b) Proposed formation of sulphates during adsorption of SO_2 on $[Cu(OH)]^+$-Al and Cu^{2+}-2Al sites. Adapted with permission from ref. [61]. (c) NH_3-SCR performance of fresh Cu-SSZ-13 (FR-Cu-SSZ-13), hydrothermally aged Cu-SSZ-13 (HA-Cu-SSZ-13) and sulphur-aged Cu-SSZ-13 (SA-Cu-SSZ-13) at high temperatures (750°C). Adapted with permission from ref. [64].

subsequently desulphated Cu-SSZ-13 catalysts [56]. The low-temperature performance was significantly inhibited on the sulphated samples compared to fresh ones, while the high-temperature performance was scarcely influenced. Thermal treatment can partially recover the deNO_x efficiency of Cu-SSZ-13 and the low-temperature activity increased with progressively higher regeneration temperatures, indicating that various S-containing species, including reversible and irreversible ones, existed on the sulphated Cu-SSZ-13 catalysts.

Low-temperature (200°C) SO_2 poisoning of Cu-SSZ-13 generally leads to the formation of H_2SO_4, $CuSO_4$ and $Al_2(SO_4)_3$ species, with different thermal stabilities [57]. The decomposition temperatures are ∼500°C, ∼630°C and ∼800°C for H_2SO_4, $CuSO_4$ and $Al_2(SO_4)_3$, respectively [57]. H_2SO_4 easily combines with NH_3 to promote the accumulation of ammonium-sulphur species under SCR conditions [57–60]. Therefore, SO_2 treatment under SCR conditions ($NH_3 + NO + O_2 + H_2O$) induced more severe deactivation compared to that in the presence of $O_2 + H_2O$ only [58]. Jangjou *et al.* found that ammonium sulphate formed on Cu^{2+}-2Al sites and could be generally regarded as a reversible deactivation due to its facile regeneration by heat treatment [61]. However, SO_2 adsorbed on $[Cu(OH)]^+$-Al sites leads to copper bisulphite species formation, which are further oxidized to form copper bisulphate with increasing temperature (Fig. 8b) [61]. The accumulation of ammonium sulphate and copper bisulphate limits the formation and mobility of $[Cu(NH_3)_2]^+$ ions that serve as dynamic active sites, thus resulting in a marked decrease in deNO_x efficiency [62,63]. The copper-sulphur species need a higher temperature (>550°C) to decompose and are thus thought to result in irreversible deactivation. $Al_2(SO_4)_3$ is difficult to decompose and regarded as an irreversible deactivation species due to the destruction of framework Al. When the SO_2-poisoning temperature increased to 400°C, more copper-sulphur species formed due to the instability of ammonium sulphate. However, 750°C sulphur aging with H_2O resulted in permanent deactivation of Cu-SSZ-13 without accumulation of reversible species, since SO_2 increased the acidity of the hydrothermal atmosphere and accelerated the destruction of the zeolite structure as well as the loss of acid sites and active Cu^{2+} species (Fig. 7c) [64]. Compared to SO_2, SO_3 poisoning is more severe due to the primary formation of copper bisulphate species, which only decompose at elevated temperatures (>550°C) [59].

Turning to the solution to SO_2 poisoning, heat treatment at elevated temperature (∼500°C), an easily accessible temperature in actual diesel exhaust, is generally an effective way to regenerate the deNO_x efficiency of Cu-SSZ-13, since most of the total deactivation is reversible. Moreover, it should be noted that some reductants, such as NH_3 and C_3H_6, can achieve the removal of sulphur species by chemical reaction without heat treatment at elevated temperatures [56,65]. Besides, Wei *et al.* found that mild HTA increased the SO_2 tolerance of Cu-SSZ-13 since some sulphur-sensitive $[Cu(OH)]^+$-Al species transformed to stable Cu^{2+}-2Al species during mild HTA [66]. Yu *et al.* found that some metal oxides, which can be mixed with Cu-SSZ-13 zeolite to form hybrid catalysts, can serve as a sacrificial component to prevent Cu^{2+} site poisoning. However, the improvement in SO_2 tolerance is still limited [67].

Effects of PO_4^{3-}, HCs and metal co-cations

The exhaust from diesel engines includes various contaminants derived from the engine, urea (NH_3 source), volatile engine oils, volatile precious metals and fuel additives; therefore, besides hydrothermal aging and sulphur poisoning there

are also other toxic species that need to be considered in diesel exhaust, such as PO_4^{3-}, HCs and alkali metals, although their quantities are small. Phosphorus mainly comes from fuels (biofuels) and some lubricating oils as well as some fuel additives. There have been several studies mainly focused on phosphorus poisoning of Cu-SSZ-13. Phosphorus poisoning is generally simulated by incipient wetness impregnation using $(NH_4)_2HPO_4$ solutions as precursors. After PO_4^{3-} loading, Cu-P species and Al-P species are formed and have been identified by many researchers [68–71]. The formation of Cu-P species induces a decrease in the NO and NH_3 oxidation of Cu-SSZ-13, which further results in a reduction in low-temperature SCR activity due to loss of active Cu^{2+} sites, but improvement in high-temperature SCR activity due to the suppression of NH_3 non-selective oxidation [68,71,72]. In detail, Wang *et al.* found that $[Cu(OH)]^+$-Al interacts more easily with phosphorus and coordinates with only one P atom (PO_3^- or PO_4^{3-}), while the poisoning of Cu^{2+}-2Al involves two P atoms (i.e. P_2O_5). The formation of Al-P species primarily influences the HTS of Cu-SSZ-13. P loading can lead to part of the phosphorus inserting into the zeolite framework to form a localized $AlPO_4$ phase, which is severe after HTA [72,73]. This indicates that P poisoning accelerates the collapse of the structure of Cu-SSZ-13 zeolite during HTA. However, Zhao *et al.* found, importantly, that an appropriate content of phosphate ions can prevent the structure collapse due to the formation of a silicoaluminophosphate interface [71]. To create conditions approaching the practical situation, Xie *et al.* simulated the vapour-phase phosphorus poisoning (using diluted H_3PO_4 solution) of Cu-SSZ-13 during NH_3-SCR operating conditions [70]. Ammonium phosphate is easily formed at low temperatures but decomposes at elevated temperatures. Unfortunately, the decomposition of ammonium phosphate still deposits P in the catalysts. At high temperatures, metaphosphate (PO_3^-) was the dominant deposited compound compared to phosphorus oxide (P_2O_5) and phosphate (PO_4^{3-}) during PO_4^{3-} poisoning under SCR conditions. In summary, PO_4^{3-} poisoning results in accumulative and permanent deactivation, although a small amount of phosphorus probably benefits the hydrothermal stability.

The effect of co-cations should also be considered since the exhaust contains some metal impurities derived from various additives, and some metals are residual species or are purposefully added in the synthetic process to improve the catalytic activity of Cu-SSZ-13. The influence of Na on Cu-SSZ-13 has been extensively studied by researchers, since Na is not only a poison but also a residual species in most synthetic methods. We first investigated the effect of Na^+ on one-pot synthesized Cu-SSZ-13 and basically found that the presence of Na^+ decreased the catalytic activity and hydrothermal stability [74]. However, Gao *et al.* found that Na^+, as well as Li^+ and K^+, promoted the low-temperature SCR rate and HTS of Cu-SSZ-13 [75,76]. Zhao also found that an appropriate Na^+ content could increase both the low-temperature activity and hydrothermal stability of their organotemplate-free synthesized Cu-SSZ-13 [77]. The primary reason for the discrepancy is varying Cu contents in the Cu-SSZ-13 catalysts. Na^+, located at ion-exchange sites, weakens interactions between Cu^{2+} and the zeolite framework and promotes some Cu^{2+} accumulation during HTA, which is more pronounced in the one-pot synthesized Cu-SSZ-13 with high Cu content due to the low Si/Al ratio (∼4.2). However, if the Cu content is suitable, the weakened interaction with the zeolite framework makes Cu^{2+} more reducible, and a moderate amount of Na^+ can prevent zeolite dealumination and stabilize the framework during HTA. Analogously, among rare earth co-cations, moderate amounts of Ce and Y ions, which locate at ion-exchange sites, were found to improve the HTS of Al-rich Cu-SSZ-13 [78–81]. Other metal co-cations (such as Cs^+, Ca^{2+} Mg^{2+} etc.) generally showed a poisoning effect on Cu-SSZ-13 since they destabilized isolated Cu ions via site competition [76,82]. In summary, some co-cations have a positive effect on Cu-SSZ-13, but controlling the content of Cu ions and co-cations is the key factor.

Hydrocarbon species are primarily formed due to insufficient combustion of fuel during cold-start oxidation or when the upstream DOC is aged. Basically, heavy HCs such as $C_{10}H_{22}$ and $C_{12}H_{26}$ have no effect on the deNO_x efficiency of Cu-SSZ-13, since the small channel (∼3.8 Å) prevents the long-chain HC molecules from entering into the zeolite [83,84]. As for light HCs, Cu-SSZ-13 shows a slight decrease in NO conversion in the presence of C_3H_6 in the medium temperature range (200–400°C). In this temperature range, C_3H_6 is partially oxidized and forms some carbonaceous deposits, resulting in a decrease in NO conversion [83,85]. When the temperature is above 400°C, the deposited carbon burns off and C_3H_6-SCR can also occur, so that the NO_x conversion is only slightly changed [85–87]. When the temperature is below 200°C, there is also no adverse impact of C_3H_6 since the energy is insufficient to propel the C_3H_6 molecule (with a kinetic diameter of ∼4.5 Å) into the pores [85].

Synthetic methodology

The availability of an efficient, economical and environmentally friendly synthetic method is vitally important for the practical application of Cu-SSZ-13. In the synthesis process, the temperature, seeds and template all influence the space-time yields (STY) of CHA zeolite. Generally, Cu-SSZ-13 catalysts are prepared by an ion-exchange method, with the SSZ-13 substrate synthesized using N,N,N-trimethyl-1-adamantammonium hydroxide (TMAdaOH) as a template [88]. In consideration of the low STY (160°C for 90–120 h), high price of TMAdaOH, and complex ion-exchange process, many new synthetic methods were developed by researchers. Han *et al.* used coal gangue as the Al source and shortened the nucleation time of SSZ-13 to 7 h in the presence of TMAdaOH, but 36 h was still needed to prepare SSZ-13 with high crystallinity [89]. Wang *et al.* used a solvent-free method to successfully synthesize SSZ-13 substrate by using economical N,N,N-dimethylethylcyclohexylammonium bromide (DMCHABr) as an organic template to achieve 95.7% of efficiency of silica source usage. Interestingly, the Cu^{2+} ion-exchanged SSZ-13 synthesized using DMCHABr as a template showed higher HTS than Cu-SSZ-13 synthesized by the traditional method using TMAdaOH as a template, since more spatially close Al sites (favouring Cu^{2+}-2Z as elaborated in 'Hydrothermal stability' section) exist in the former Cu-SSZ-13 [20,90]. Furthermore, seed-assisted rapid synthesis of SSZ-13 through interzeolite transformation from FAU zeolite was achieved in the absence of solvent, which shortened the crystallization time to 1 day [91]. Simultaneously, the solvent-free conditions benefit the stability of the TMAdaOH template at high temperatures (>200°C), so that Bian *et al.* shortened the synthetic time of SSZ-13 to only 1.5 h (extremely high STY) at 240°C. Besides DMCHABr, Chen *et al.* used economical choline chloride (CC) as a template to synthesize the SSZ-13 substrate [92]. Furthermore, they optimized this method with the assistance of fluoride and seeds, resulting in crystallinity similar to that of a sample synthesized using TMAdaOH [93]. Moreover, through the utilization of CHA seeds, an organotemplate-free synthesis of SSZ-13 was developed by Zhao *et al.* [77]. After Cu^{2+} ion-exchange, this Cu-SSZ-13 sample showed excellent catalytic activity, with NO_x conversion higher than 90% in the temperature range 200–500°C, but at relatively low GHSV (80 000 h^{-1}).

The product synthesized by all the above methods is the SSZ-13 substrate, which subsequently needs multiple steps to obtain Cu-SSZ-13 catalysts, at least including calcination, NH_4^+ ion-exchange, Cu^{2+} ion-exchange and calcination again. Therefore, a direct synthesis method for Cu-SSZ-13 catalyst is desired. Xiao and co-workers first directly synthesized Cu-SSZ-13 by using Cu-tetraethylenepentamine (Cu-TEPA) as a template to introduce the copper species *in situ* (Fig. 9a) [94]. Nevertheless, using Cu-TEPA as the sole template easily led to the formation of accumulation of CuO_x clusters, which is detrimental to HTS and high-temperature activity (Fig. 9b, black line). Therefore, a series of aftertreatments were developed by our group to optimize the structure and copper species of *in situ* synthesized Cu-SSZ-13 [51,74,86]. We found that synergetic treatment by HNO_3 and NH_4NO_3, which can accurately tune the framework crystallinity and copper state and content, markedly increased the SCR activity and hydrothermal stability (Fig. 9b, red line). Since Cu-SSZ-13 was first reported to have excellent NH_3-SCR activity and hydrothermal stability in 2010, researchers have studied the physiochemical properties of Cu-SSZ-13 in detail and optimized the Si/Al ratio to ∼12 from 17.5 [48,95], and we believe that the Si/Al of Cu-SSZ-13 can be lowered further. It should be noted that the *in situ* synthesized Cu-SSZ-13 (Fig. 9c) showed activity superior to commercial Cu-SSZ-13 (Fig. 9d, Si/Al∼12), especially at high temperatures. This is because the *in situ* synthesized Cu-SSZ-13 is an Al-rich zeolite, which accommodates large amounts of paired framework Al for stable coordination of Cu^{2+}-2Al (see details in 'Copper species' section), thus leading to high deNO_x efficiency and HTS.

OTHER SMALL-PORE ZEOLITES APPLIED TO NH_3-SCR

Shape selectivity of small-pore structure in NH_3-SCR reaction

Cu-SSZ-13 is a Cu-exchanged small-pore zeolite with the CHA crystal structure, which contains a channel opening of about 3.8 × 3.8 Å (8MR) and a large CHA cage. As stated above, this specific structure is closely related to the properties of Cu-SSZ-13 catalysts in the NH_3-SCR reaction. For example, the dealumination process of small-pore zeolites during HTA is inhibited because the constricting dimensions of the small pores limits the detachment of aluminium hydroxide [45,96]. The small-pore structure restricts large hydrocarbon species from entering the pores of the catalysts during the SCR reactions,

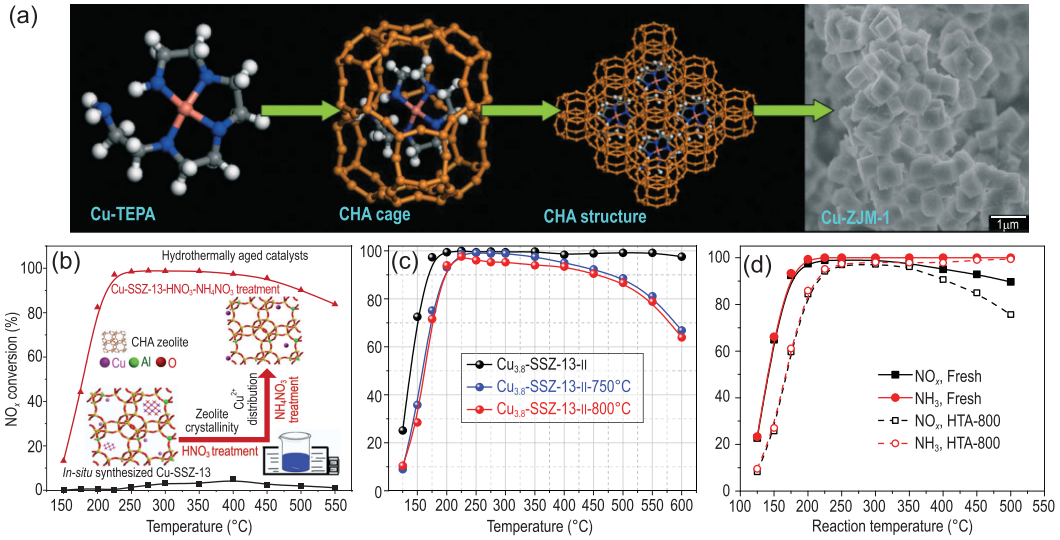

Figure 9. (a) Mechanism of preparation of Cu-TEPA templated Cu-SSZ-13 zeolites. Adapted with permission from ref. [94]. (b) HNO_3-NH_4NO_3 aftertreatment of *in situ* synthesized Cu-SSZ-13. (c) NH_3-SCR performance of aftertreated Cu-SSZ-13 before and after hydrothermal aging at 750 and 800°C, GHSV = 200 000 h^{-1}. Adapted with permission from ref. [51]. (d) NH_3-SCR performance of commercial fresh and HTA-800 Cu/SSZ-13 samples (Si/Al = 12, Cu loading = 2.1%), GHSV = 200 000 h^{-1}. Adapted with permission from ref. [48].

so that Cu-SSZ-13 possesses good hydrocarbon tolerance, especially towards long-chain HCs [45]. The small-pore Cu-CHA zeolite showed very slow N_2O formation in the NH_3-SCR reaction because the small-pore structure can stabilize NH_4NO_3 [38]. Moreover, the formation of dynamic binuclear Cu ions can be achieved in the large CHA cage. Therefore, the HTS, poisoning resistance, catalytic selectivity and activity, and reaction mechanism are closely related to the shape selectivity of the SSZ-13 structure.

Based on the shape selectivity of the Cu-SSZ-13 catalyst, here, we summarize the essential characteristics of Cu-based small-pore zeolites with excellent activity and hydrothermal stability: (i) The 8MR pore structure is extremely important to its HTS due to its inhibiting effect on dealumination. Moreover, NH_3-SCR reactants with small volume go through the 8MR easily while some large poisons (such as long-chain HCs) are prevented from entering the zeolite. (ii) A suitable elemental composition offers plenty of ion-exchangeable sites and Brønsted sites as well as a stable skeleton. (iii) The large cage-type structure (CHA cage of SSZ-13) provides a reaction zone where a large molecule such as dynamic $Cu(NH_3)_2^+$ can favourably combine to form dinuclear active sites to complete the O_2 activation. Based on the above principles, researchers have surveyed the zeolite family, and some typical small-pore zeolites with comparable deNO$_x$ efficiency or/and HTS to Cu-SSZ-13 were developed.

Hydrothermally stable small-pore zeolites

Utilization of the Cu-SSZ-39 zeolite catalyst with AEI structure for the SCR of NO$_x$ was first reported by Moliner *et al.* [97]. The difference between the AEI and CHA structures is the connection mode of the D6Rs. The neighbouring D6Rs have mirror symmetry in AEI, while they are arranged in parallel in CHA, resulting in different channels and cavities. Recently, we compared the NH_3-SCR activity and HTS of Al-rich Cu-SSZ-39 and Cu-SSZ-13 and found that Cu-SSZ-39 showed higher hydrothermal stability but lower deNO$_x$ efficiency (Fig. 10a), and both of them showed excellent N_2 selectivity, with N_2O production less than 10 ppm [98]. It was found that SSZ-39 contained more paired Al, which favoured the formation of stable Cu^{2+}-2Al species, resulting in higher stability for active sites but lower deNO$_x$ efficiency compared to $[Cu(OH)]^+$-Al. In another aspect, SSZ-39 has a more tortuous channel structure than SSZ-13 does (Fig. 10b). This structure can inhibit the detached $Al(OH)_3$ from exiting the pores of the AEI zeolite framework, which would result in reincorporation of $Al(OH)_3$ into the framework when the catalyst cools down. However, the tortuous channel is adverse to the mobility of active $Cu(NH_3)^+$ species, which further reduces the deNO$_x$ efficiency [98]. Furthermore, we investigated the SO_2, alkali and alkaline earth metal resistance of Cu-SSZ-39 for NH_3-SCR. Similar to Cu-SSZ-13, Cu-SSZ-39

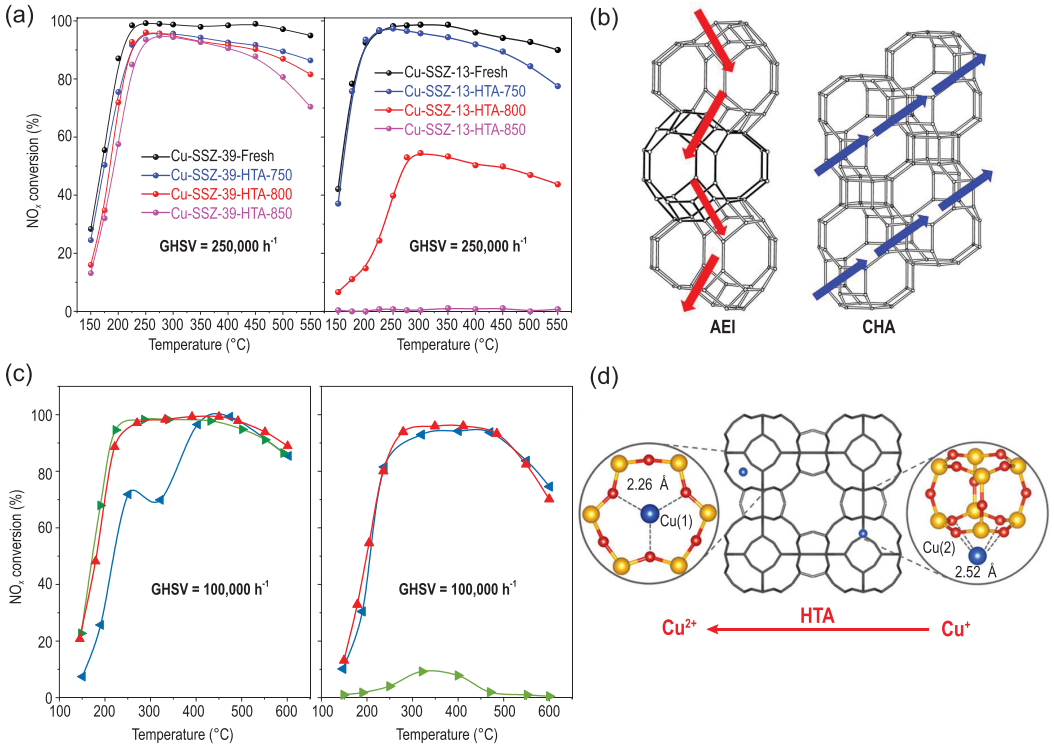

Figure 10. (a) Comparative NH_3-SCR performance of Cu-SSZ-39 and Cu-SSZ-13 before and after hydrothermal aging. (b) Channel structures of AEI and CHA zeolites. Adapted with permission from ref. [98]. (c) NH_3-SCR performance of Cu-LTA-16–0.48 (red), Cu-LTA-11–0.48 (green) and Cu-LTA-23–0.5 (blue) before (left) and after (right) hydrothermal aging at 900°C. Adapted with permission from ref. [104]. (d) Copper species at different locations and transformation between the two copper species during HTA. Adapted with permission from ref. [105].

also showed reversible (H_2SO_4) and irreversible ($CuSO_4$) deactivation after SO_2 poisoning. Regeneration at 600°C can recover most of the NH_3-SCR activity, but decomposition of $CuSO_4$ needs a higher temperature [99]. However, the catalytic activity and HTS were significantly decreased after alkali/alkaline earth poisoning due to the deterioration of the zeolite structure and CuO_x formation from isolated Cu^{2+}, which still should be optimized and improved [100]. To further increase the hydrothermal stability of Cu-SSZ-39, Sano and co-workers used tetraethylphosphonium (TEP) cations as a structure-directing agent to obtain P-modified Cu-SSZ-39 with excellent hydrothermal stability (hydrothermal treatment at 900°C for 4 h). However, fluoride, which is an environmental pollutant and harmful to human health, was required to accelerate mineralization, and NO conversion decreased with increasing P/Al ratio [101]. Martin *et al.* used N,N-dimethyl-3,5-dimethylpiperidinium and Cu-TEPA as dual OSDAs to directly synthesize Cu-SSZ-39, which showed good NH_3-SCR performance, but HTS was not tested [102]. Moreover, given that SSZ-39 has traditionally been synthesized through interzeolite transformation from high-silica Y, of which the preparation is expensive and requires complex post-treatments, Xu *et al.* successfully synthesized SSZ-39 through interzeolite transformation from low-cost and widely used ZSM-5 and beta zeolites [103]. In summary, Cu-SSZ-39 zeolite exhibits strong potential as an NH_3-SCR catalyst for actual application due to its optimal deNO_x efficiency and outstanding hydrothermal stability.

Besides Cu-SSZ-39, high silica Cu-LTA is another highly stable zeolite for the NH_3-SCR reaction. It was first reported by Hong *et al.* that fully copper-exchanged high-silica LTA zeolite possessed excellent hydrothermal stability during the NH_3-SCR reaction. Even after hydrothermal aging at 900°C, the samples still showed good NO_x conversion (Fig. 10c), under which conditions the Cu-SSZ-13 structure collapsed [104]. Furthermore, an increase in the low-temperature standard NH_3-SCR activity was found on Cu-LTA with Si/Al of 23 and Cu/Al of 0.5 after hydrothermal aging. They ascribed this to the transformation of inactive Cu^+ ions in the sod cage coordinated to four-rings to active Cu^{2+} ions in the single 6-rings (s6r) centre (Fig. 10d) [105]. In addition, Wang *et al.* found that HTA prompted the CuO_x and Cu^{2+} to transform to $Cu(OH)^+$ species on a Cu/LTA catalyst

prepared by the incipient wetness impregnation (IWI) method, which is opposite to the behaviour of Cu-SSZ-13 [106]. Another aspect that is different from Cu-SSZ-13 is the promotion effect on NO_x conversion of Cu-LTA under FSCR conditions [106,107]. Ryu *et al.* found that both Cu^{2+} and $Cu(OH)^+$ in Cu-LTA are substantially centred on the single six-rings, where the reactant molecules should be less accessible than the eight-ring window sites, resulting in lower amounts of ammonia nitrate compared to that produced in Cu-SSZ-13 [107]. Regarding the effect of SO_2, the $Cu(OH)^+$ species in this catalyst were found to be more vulnerable to SO_2 poisoning due to their weak interaction with the zeolite framework structure compared to those in Cu-SSZ-13. Nevertheless, the fresh $deNO_x$ efficiency of Cu-LTA can be totally recovered by regeneration at the elevated temperature of 750°C [108]. Although Cu-LTA zeolite showed extraordinary HTS, relatively optimized FSCR performance as well as good SO_2 tolerance, the synthesis of Cu-LTA should continue to be explored in future due to the requirement of F^- addition in the synthetic process [109,110].

Other alternative small-pore zeolites

Besides AEI and LTA zeolites, there are also some other small-pore zeolites that should be given attention, as shown in Table S1. The highly crystalline KFI-type zeolite was successfully synthesized via transformation of FAU-type zeolite with Na^+ and K^+ ions in the absence of an organic SDA (OSDA) [111]. The Cu ion-exchanged KFI catalyst showed good NH_3-SCR activity and HTS, which, however, was still inferior to that of Cu-SSZ-13 [111]. Nevertheless, Han *et al.* synthesized high-silica Cu-KFI with $Si/Al > 5$ by only using K^+ as a directing agent, which is more sustainable for zeolite synthesis [112]. Importantly, the high-silica Cu-KFI showed excellent HTS and maintained NO_x conversion of ∼57% at 200°C even after HTA at 800°C [112]. Cu-SSZ-50 with the RTH structure, which has 2D channels with aperture sizes of 0.41 nm × 0.38 nm (8MRs) and 0.56 nm × 0.25 nm (distorted 8MRs), also showed comparable NH_3-SCR activity but relatively low hydrothermal stability [113,114]. Highly active α species and inert β species both existed in Cu-SSZ-50 with high Cu loading, but the α species were easily movable and transferred to more stable sites during HTA [114]. Cu-SSZ-50 can be synthesized at high temperatures in less than 1 hour [115], which gives it significant potential for application in NH_3-SCR as long as the hydrothermal stability can be improved in future. Martin *et al.* have investigated various cage-based small-pore catalysts, among which Cu-AFX and Cu-ERI were the first to be applied in the NH_3-SCR reaction. However, although they have similar small-pore structures to Cu-SSZ-13, the SCR activity and HTS still need improvement [116]. Through transformation of FAU zeolite in the presence of an alkali metal-crown ether (AMCE) complex and RHO seeds, Ke *et al.* prepared high-silica RHO zeolite with Si/Al of 7.6. The copper ion-exchanged RHO catalyst showed good NH_3-SCR performance with relatively high HTS at 800°C [117].

In fact, zeolites with small-pore structures and adequate ion-exchange sites have great potential for utilization as NH_3-SCR catalysts with high $deNO_x$ efficiency and hydrothermal stability. Researchers have developed many small-pore zeolites in the past several years as discussed above. These zeolites, however, still require comprehensive and systematic in-depth study as well as optimization of physicochemical properties before their practical implementation. Also, it is important that the synthetic method for these developed zeolites is efficient, economical and environmentally friendly. In another aspect, moreover, development of the new type small-pore zeolites with high SCR activity and HTS is still worthwhile based on the design principles proposed above, since there is still considerable room in the small-pore zeolite family for researchers to investigate [118]. Therefore, research should still be devoted to developing and improving small-pore zeolites in the future.

SUMMARY AND PERSPECTIVE

General conclusion

This survey provides an easy-to-read and systematic overview of the reported Cu-based small-pore zeolites applied to the NH_3-SCR reaction in the past decade. Using Cu-SSZ-13 as the main example, we presented an overview of the standard and fast SCR mechanisms, hydrothermal stability, chemical poisoning mechanism (SO_2, PO_4^{3-}, HCs, alkali and alkaline earth metals), co-cation effects and synthetic methodology. The discovery of the locally homogenous reaction mechanism (SSCR) is a big step forward in the field of catalytic chemistry. This catalytic reaction mechanism will help researchers rationally design catalysts with dynamic active sites in order to achieve high catalytic activity. For actual application of Cu-SSZ-13, the hydrothermal stability and chemical poisoning tolerance should be improved by carefully tuning the properties in the initial synthetic process and/or post-treatment. By precisely controlling the type and amount of co-cation metals, the SCR activity and hydrother-

mal stability can be improved. Economical and environmentally friendly synthesis routes for the zeolites mainly include the *in situ* method, solvent-free method and template-free method, as well as combinations of these. Each method can achieve sustainable development by using rational and economical raw materials. In addition, the unique properties of other small-pore zeolites, especially AEI- and LTA-type zeolites, were also summarized. Cu-AEI and Cu-LTA zeolites showed hydrothermal stability superior to that of Cu-SSZ-13 under certain conditions, while further breakthroughs still need to be made, such as green and sustainable synthetic methods for these other small-pore zeolites.

Opportunities

As we pointed out in the introduction section, the typical properties of Cu-exchanged small-pore zeolites match perfectly with the required characteristics of NH_3-SCR catalysts, resulting in excellent deNO_x efficiency in the NH_3-SCR reaction. First, the dual-functional Cu^{2+} ion, as both redox and acid site, achieves the limiting case of tight coupling for redox-acid sites in NH_3-SCR catalysts. Second, the atomic-level dispersal of Cu^{2+} also reaches the limits of high dispersion of active sites in NH_3-SCR catalysts. Last but not least, the dynamic active sites for the copper-ammonia complex, which is mobile in the zeolite cage, adequately expose them to the reactants. The above three points determine the excellent NH_3-SCR activity of Cu^{2+}-exchanged zeolites. Besides, the shape selectivity of the small-pore structure guarantees its high hydrothermal stability and poisoning resistance. In one aspect, the narrow small pores limit the diffusion of hydrolysed $Al(OH)_3$ and accumulation of Cu^{2+}, resulting in outstanding hydrothermal stability of framework and active Cu^{2+} sites. In another aspect, some long-chain HCs and large poisoning molecules are prevented from access to the active sites. Therefore, Cu-based small-pore zeolites represent an immense opportunity as efficient and stable NH_3-SCR catalysts.

In actual application, the consumption of diesel and jet fuel in 2040 will increase 75% compared with that in 2010. Therefore, diesel engines will be irreplaceable as the primary power source for the freight, navigation and marine engine industries and non-road engineering machinery for the foreseeable future, for which saving energy and restraining emissions will be the greatest challenges. Increasingly stringent emission standards are being developed across the world to reduce polluting emissions from diesel engines. In the US, the technological feasibility of achieving an emission limit of 0.02 g/bhp-hr and Low Load Cycle (LLC) limit below 0.075 g/bhp-hr has been demonstrated. In China, highway freight reached ∼40 billion tonnes, accounting for 76.9% of the total freight [5]. The China VI Standards for emissions from diesel-fuelled heavy-duty vehicles will be fully implemented on 1 July 2021. The standard explicitly forbids leakage of V-containing complexes into the atmosphere during the lifetime of vehicles that utilize the V-based SCR catalyst, which indicates that the V-based catalyst will not be applicable for exhaust purification in the future. As an alternative, the development of Cu-based small-pore zeolites with high activity and stability is of vital importance.

Challenges

Despite the great opportunities offered by Cu-based small-pore zeolites, there are still some challenges to be addressed.

(i) The chemical poisoning tolerance (SO_2, P and alkali metals etc.) should be improved. For example, although thermal treatment can recover most of the deNO_x efficiency of S-poisoned zeolite-based catalysts, steady-state SO_2 poisoning results in a significant decrease due to the formation of ammonium sulphate and copper bisulphite. The addition of other metals as sacrificial components is a possible way to increase the SO_2 resistance. The small HCs poisoning in the medium temperature range should also be improved in future.

(ii) Although the abnormal FSCR reaction has scarcely any positive effect on the deNO_x efficiency over Cu-based small-pore zeolites, NO_2 is always present due to the partial oxidation of NO in the DOC part. Therefore, the NO_x reduction pathway in the presence of NO_2 is still worth investigating. The atomic-level understanding of the abnormal FSCR reaction process is still worthy of study, by suitable experiments accompanied by auxiliary calculations.

(iii) Besides CHA-, LTA- and AEI-type zeolites, development of other small-pore zeolites with suitable elemental composition and pore structure for the NH_3-SCR reaction, which can be attractive alternative candidates for future NH_3-SCR catalysts, should be pursued.

(iv) The green and sustainable synthesis of small-pore zeolites is important for actual application. Although some economical and environmentally friendly methods to synthesize Cu-SSZ-13 have been reported, they each have advantages and disadvantages. It is urgently necessary to combine the advantages of these methods, such as by combination of *in situ*,

solvent-free and template-free methods. Green and sustainable routes for synthesizing LTA and AEI also need to be addressed in the future. Moreover, the development of ultrafast synthesis methods with various assistive technologies (such as microwave heating or seeded growth) to increase efficiency and reduce the cost is of great importance for industrial application.

SUPPLEMENTARY DATA

Supplementary data are available at *NSR* online.

FUNDING

This work was supported by the National Natural Science Foundation of China (21637005, 21906172, 51822811 and 51978640).

Conflict of interest statement. None declared.

REFERENCES

1. Sun Q, Xie Z and Yu J *et al.* The state-of-the-art synthetic strategies for SAPO-34 zeolite catalysts in methanol-to-olefin conversion. *Natl Sci Rev* 2018; **5**: 542–58.
2. Xie Z, Liu Z and Wang Y *et al.* Applied catalysis for sustainable development of chemical industry in China. *Natl Sci Rev* 2015; **2**: 167–82.
3. Zhang R, Liu N and Lei Z *et al.* Selective transformation of various nitrogen-containing exhaust gases toward N_2 over zeolite catalysts. *Chem Rev* 2016; **116**: 3658–721.
4. Zheng B, Tong D and Li M *et al.* Trends in China's anthropogenic emissions since 2010 as the consequence of clean air actions. *Atmos Chem Phys* 2018; **18**: 14095–111.
5. Ministry of Ecology and Environment of the People's Republic of China. *China Mobile Source Environmental Management Annual Report 2020*. http://www.mee.gov.cn/xxgk2018/xxgk/xxgk15/202008/t20200810˙793252.html (10 February 2021, date last accessed).
6. Qu W, Liu X and Chen J *et al.* Single-atom catalysts reveal the dinuclear characteristic of active sites in NO selective reduction with NH_3. *Nat Commun* 2020; **11**: 1532–8.
7. Shan W, Yu Y and Zhang Y *et al.* Theory and practice of metal oxide catalyst design for the selective catalytic reduction of NO with NH_3. *Catal Today* 2020; doi: 10.1016/j.cattod.2020.05.015.
8. Liu F, Yu Y and He H. Environmentally-benign catalysts for the selective catalytic reduction of NO_x from diesel engines: structure-activity relationship and reaction mechanism aspects. *Chem Commun* 2014; **50**: 8445–63.
9. Bull I, Xue WM and Burk P *et al.* Copper CHA zeolite catalysts. US Patent 7,610,662, 2009.
10. Kwak JH, Tonkyn RG and Kim DH *et al.* Excellent activity and selectivity of Cu-SSZ-13 in the selective catalytic reduction of NO_x with NH_3. *J Catal* 2010; **275**: 187–90.
11. Kwak JH, Tran D and Burton SD *et al.* Effects of hydrothermal aging on NH_3-SCR reaction over Cu/zeolites. *J Catal* 2012; **287**: 203–9.
12. Paolucci C, Khurana I and Parekh AA *et al.* Dynamic multinuclear sites formed by mobilized copper ions in NO_x selective catalytic reduction. *Science* 2017; **357**: 898–903.
13. Fickel DW and Lobo RF. Copper coordination in Cu-SSZ-13 and Cu-SSZ-16 investigated by variable-temperature XRD. *J Phys Chem C* 2010; **114**: 1633–40.
14. Korhonen ST, Fickel DW and Lobo RF *et al.* Isolated Cu^{2+} ions: active sites for selective catalytic reduction of NO. *Chem Commun* 2011; **47**: 800–2.
15. Kwak JH, Zhu H and Lee JH *et al.* Two different cationic positions in Cu-SSZ-13? *Chem Commun* 2012; **48**: 4758–60.
16. Andersen CW, Bremholm M and Vennestrom PN *et al.* Location of Cu^{2+} in CHA zeolite investigated by X-ray diffraction using the Rietveld/maximum entropy method. *IUCrJ* 2014; **1**: 382–6.
17. Paolucci C, Parekh AA and Khurana I *et al.* Catalysis in a cage: condition-dependent speciation and dynamics of exchanged Cu cations in SSZ-13 zeolites. *J Am Chem Soc* 2016; **138**: 6028–48.
18. Di Iorio JR and Gounder R. Controlling the isolation and pairing of aluminium in chabazite zeolites using mixtures of organic and inorganic structure-directing agents. *Chem Mater* 2016; **28**: 2236–47.
19. Di Iorio JR, Nimlos CT and Gounder R. Introducing catalytic diversity into single-site chabazite zeolites of fixed composition via synthetic control of active site proximity. *ACS Catal* 2017; **7**: 6663–74.
20. Zhang J, Shan Y and Zhang L *et al.* Importance of controllable Al sites in CHA framework by crystallization pathways for NH_3-SCR reaction. *Appl Catal B* 2020; **277**: 119193–200.
21. Borfecchia E, Lomachenko KA and Giordanino F *et al.* Revisiting the nature of Cu sites in the activated Cu-SSZ-13 catalyst for SCR reaction. *Chem Sci* 2015; **6**: 548–63.
22. Gao F, Mei D and Wang Y *et al.* Selective catalytic reduction over Cu/SSZ-13: linking homo- and heterogeneous catalysis. *J Am Chem Soc* 2017; **139**: 4935–42.
23. Lomachenko KA, Borfecchia E and Negri C *et al.* The Cu-CHA deNO_x catalyst in action: temperature-dependent NH_3-assisted selective catalytic reduction monitored by operando XAS and XES. *J Am Chem Soc* 2016; **138**; 12025–8.
24. Moreno-González M, Hueso B and Boronat M *et al.* Ammonia-containing species formed in Cu-chabazite as per in situ EPR, solid-state NMR, and DFT calculations. *J Phys Chem Lett* 2015; **6**: 1011–7.
25. Martini A, Borfecchia E and Lomachenko KA *et al.* Composition-driven Cu-speciation and reducibility in Cu-CHA zeolite catalysts: a multivariate XAS/FTIR approach to complexity. *Chem Sci* 2017; **8**: 6836–51.
26. Fahami AR, Günter T and Doronkin DE *et al.* The dynamic nature of Cu sites in Cu-SSZ-13 and the origin of the seagull NO_x conversion profile during NH_3-SCR. *React Chem Eng* 2019; **4**: 1000–18.

27. Gao F, Walter ED and Kollar M *et al.* Understanding ammonia selective catalytic reduction kinetics over Cu/SSZ-13 from motion of the Cu ions. *J Catal* 2014; **319**: 1–14.
28. Paolucci C, Verma AA and Bates SA *et al.* Isolation of the copper redox steps in the standard selective catalytic reduction on Cu-SSZ-13. *Angew Chem Int Ed* 2014; **126**: 12022–7.
29. Hammershøi PS, Negri C and Berlier G *et al.* Temperature-programmed reduction with NO as a characterization of active Cu in Cu-CHA catalysts for NH_3-SCR. *Catal Sci Technol* 2019; **9**: 2608–19.
30. Chen L, Falsig H and Janssens TVW *et al.* Effect of Al-distribution on oxygen activation over Cu–CHA. *Catal Sci Technol* 2018; **8**: 2131–6.
31. Negri C, Selleri T and Borfecchia E *et al.* Structure and reactivity of oxygen-bridged diamino dicopper (II) complexes in Cu-CHA catalyst for NH_3-SCR. *J Am Chem Soc* 2020; **142**: 15884–96.
32. Chen L, Janssens TVW and Vennestrøm PNR *et al.* A complete multisite reaction mechanism for low-temperature NH_3-SCR over Cu-CHA. *ACS Catal* 2020; **10**: 5646–56.
33. Luo J, Gao F and Kamasamudram K *et al.* New insights into Cu/SSZ-13 SCR catalyst acidity. Part I: nature of acidic sites probed by NH_3 titration. *J Catal* 2017; **348**: 291–9.
34. Janssens TVW, Falsig H and Lundegaard LF *et al.* A consistent reaction scheme for the selective catalytic reduction of nitrogen oxides with ammonia. *ACS Catal* 2015; **5**: 2832–45.
35. Kwak JH, Tran D and Szanyi J *et al.* The effect of copper loading on the selective catalytic reduction of nitric oxide by ammonia over Cu-SSZ-13. *Catal Lett* 2012; **142**: 295–301.
36. Xie L, Liu F and Liu K *et al.* Inhibitory effect of NO_2 on the selective catalytic reduction of NO_x with NH_3 over one-pot-synthesized Cu–SSZ-13 catalyst. *Catal Sci Technol* 2014; **4**: 1104–10.
37. Shan Y, Shi X and He G *et al.* Effects of NO_2 addition on the NH_3-SCR over small-pore Cu–SSZ-13 zeolites with varying Cu loadings. *J Phys Chem C* 2018; **122**: 25948–53.
38. Chen HY, Wei Z and Kollar M *et al.* A comparative study of N_2O formation during the selective catalytic reduction of NO_x with NH_3 on zeolite supported Cu catalysts. *J Catal* 2015; **329**: 490–8.
39. Kubota H, Liu C and Toyao T *et al.* Formation and reactions of NH_4NO_3 during transient and steady-state NH_3-SCR of NO_x over H-AFX zeolites: spectroscopic and theoretical studies. *ACS Catal* 2020; **10**: 2334–44.
40. Li S, Zheng Y and Gao F *et al.* Experimental and computational interrogation of fast SCR mechanism and active sites on H-Form SSZ-13. *ACS Catal* 2017; **7**: 5087–96.
41. Shan Y, Sun Y and Du J *et al.* Hydrothermal aging alleviates the inhibition effects of NO_2 on Cu-SSZ-13 for NH_3-SCR. *Appl Catal B* 2020; **275**: 119105.
42. Bendrich M, Scheuer A and Hayes RE *et al.* Unified mechanistic model for Standard SCR, Fast SCR, and NO_2 SCR over a copper chabazite catalyst. *Appl Catal B* 2018; **222**: 76–87.
43. Bendrich M, Scheuer A and Hayes RE *et al.* Increased SCR performance of Cu-CHA due to ammonium nitrate buffer: experiments with oscillating NO/NO_2 ratios and application to real driving cycles. *Appl Catal B* 2020; **270**: 118763.
44. McEwen JS, Anggara T and Schneider WF *et al.* Integrated operando X-ray absorption and DFT characterization of Cu–SSZ-13 exchange sites during the selective catalytic reduction of NO_x with NH_3. *Catal Today* 2012; **184**: 129–44.
45. Fickel DW, D'Addio E and Lauterbach JA *et al.* The ammonia selective catalytic reduction activity of copper-exchanged small-pore zeolites. *Appl Catal B* 2011; **102**: 441–8.
46. Kim YJ, Lee JK and Min KM *et al.* Hydrothermal stability of CuSSZ13 for reducing NO_x by NH_3. *J Catal* 2014; **311**: 447–57.
47. Han S, Ye Q and Cheng S *et al.* Effect of the hydrothermal aging temperature and Cu/Al ratio on the hydrothermal stability of CuSSZ-13 catalysts for NH_3-SCR. *Catal Sci Technol* 2017; **7**: 703–17.
48. Song J, Wang Y and Walter ED *et al.* Toward rational design of Cu/SSZ-13 selective catalytic reduction catalysts: implications from atomic-level understanding of hydrothermal stability. *ACS Catal* 2017; **7**: 8214–27.
49. Zhang Y, Peng Y and Li J *et al.* Probing active-site relocation in Cu/SSZ-13 SCR catalysts during hydrothermal aging by in situ EPR spectroscopy, kinetics studies, and DFT calculations. *ACS Catal* 2020; **10**: 9410–9.
50. Han S, Cheng J and Zheng C *et al.* Effect of Si/Al ratio on catalytic performance of hydrothermally aged Cu-SSZ-13 for the NH_3-SCR of NO in simulated diesel exhaust. *Appl Surf Sci* 2017; **419**: 382–92.
51. Shan Y, Du J and Yu Y *et al.* Precise control of post-treatment significantly increases hydrothermal stability of *in-situ* synthesized cu-zeolites for NH_3-SCR reaction. *Appl Catal B* 2020; **266**: 118655.
52. Ye X, Schmidt J and Wang RP *et al.* Deactivation of Cu-exchanged automotive emissions NH_3-SCR catalysts elucidated with nanoscale resolution using scanning transmission X-ray microscopy. *Angew Chem Int Ed* 2020; **132**: 15740–7.
53. Albarracin-Caballero JD, Khurana I and Di Iorio JR *et al.* Structural and kinetic changes to small-pore Cu-zeolites after hydrothermal aging treatments and selective catalytic reduction of NO_x with ammonia. *React Chem Eng* 2017; **2**: 168–79.
54. Schmidt JE, Oord R and Guo W *et al.* Nanoscale tomography reveals the deactivation of automotive copper-exchanged zeolite catalysts. *Nat Commun* 2017; **8**: 1666.
55. Ma Y, Wu X and Cheng S *et al.* Relationships between copper speciation and Brønsted acidity evolution over Cu-SSZ-13 during hydrothermal aging. *Appl Catal A* 2020; **602**: 117650.
56. Kumar A, Smith MA and Kamasamudram K *et al.* Chemical deSO_x: an effective way to recover Cu-zeolite SCR catalysts from sulfur poisoning. *Catal Today* 2016; **267**: 10–6.
57. Su W, Li Z and Zhang Y *et al.* Identification of sulfate species and their influence on SCR performance of Cu/CHA catalyst. *Catal Sci Technol* 2017; **7**: 1523–8.
58. Wijayanti K, Leistner K and Chand S *et al.* Deactivation of Cu-SSZ-13 by SO_2 exposure under SCR conditions. *Catal Sci Technol* 2016; **6**: 2565–79.
59. Hammershøi PS, Jangjou Y and Epling WS *et al.* Reversible and irreversible deactivation of Cu-CHA NH_3-SCR catalysts by SO_2 and SO_3. *Appl Catal B* 2018; **226**: 38–45.
60. Brookshear DW, Nam JG and Nguyen K *et al.* Impact of sulfation and desulfation on NO_x reduction using Cu-chabazite SCR catalysts. *Catal Today* 2015; **258**: 359–66.
61. Jangjou Y, Do Q and Gu Y *et al.* Nature of Cu active centers in Cu-SSZ-13 and their responses to SO_2. *ACS Catal* 2018; **8**: 1325–37.
62. Hammershøi PS, Jensen AD and Janssens TVW. Impact of SO_2-poisoning over the lifetime of a Cu-CHA catalyst for NH_3-SCR. *Appl Catal B* 2018; **238**: 104–10.
63. Bergman SL, Dahlin SD and Mesilov VV *et al. In-situ* studies of oxidation/reduction of copper in Cu-CHA SCR catalysts: comparison of fresh and SO_2-poisoned catalysts. *Appl Catal B* 2020; **269**: 118722–32.
64. Shan Y, Shi X and Yan Z *et al.* Deactivation of Cu-SSZ-13 in the presence of SO_2 during hydrothermal aging. *Catal Today* 2019; **320**: 84–90.

65. Ando R, Hihara T and Banno Y *et al.* Detailed mechanism of S poisoning and de-sulfation treatment of Cu-SCR catalyst. *SAE Tech Pap* 2017; 2017-01-0944.
66. Wei L, Yao D and Wu F *et al.* Impact of hydrothermal aging on SO_2 poisoning over Cu-SSZ-13 diesel exhaust SCR catalysts. *Ind Eng Chem Res* 2019; **58**: 3949–58.
67. Yu R, Zhao Z and Huang S *et al.* Cu-SSZ-13 zeolite–metal oxide hybrid catalysts with enhanced SO_2-tolerance in the NH_3-SCR of NO_x. *Appl Catal B* 2020; **269**: 118825.
68. Xie K, Leistner K and Wijayanti K *et al.* Influence of phosphorus on Cu-SSZ-13 for selective catalytic reduction of NO_x by ammonia. *Catal Today* 2017; **297**: 46–52.
69. Chen Z, Fan C and Pang L *et al.* The influence of phosphorus on the catalytic properties, durability, sulfur resistance and kinetics of Cu-SSZ-13 for NO_x reduction by NH_3-SCR. *Appl Catal B* 2018; **237**: 116–27.
70. Xie K, Wang A and Woo J *et al.* Deactivation of Cu-SSZ-13 SCR catalysts by vapor-phase phosphorus exposure. *Appl Catal B* 2019; **256**: 117815–31.
71. Zhao H, Zhao Y and Liu M *et al.* Phosphorus modification to improve the hydrothermal stability of a Cu-SSZ-13 catalyst for selective reduction of NO_x with NH_3. *Appl Catal B* 2019; **252**: 230–9.
72. Wang A, Xie K and Bernin D *et al.* Deactivation mechanism of Cu active sites in Cu/SSZ-13: phosphorus poisoning and the effect of hydrothermal aging. *Appl Catal B* 2020; **269**: 118781–92.
73. Xie K, Woo J and Bernin D *et al.* Insights into hydrothermal aging of phosphorus-poisoned Cu-SSZ-13 for NH_3-SCR. *Appl Catal B* 2019; **241**: 205–16.
74. Xie L, Liu F and Shi X *et al.* Effects of post-treatment method and Na co-cation on the hydrothermal stability of Cu–SSZ-13 catalyst for the selective catalytic reduction of NO_x with NH_3. *Appl Catal B* 2015; **179**: 206–12.
75. Gao F, Wang Y and Washton NM *et al.* Effects of alkali and alkaline earth cocations on the activity and hydrothermal stability of Cu/SSZ-13 NH_3-SCR catalysts. *ACS Catal* 2015; **5**: 6780–91.
76. Cui Y, Wang Y and Mei D *et al.* Revisiting effects of alkali metal and alkaline earth co-cation additives to Cu/SSZ-13 selective catalytic reduction catalysts. *J Catal* 2019; **378**: 363–75.
77. Zhao Z, Yu R and Zhao R *et al.* Cu-exchanged Al-rich SSZ-13 zeolite from organotemplate-free synthesis as NH_3 -SCR catalyst: effects of Na^+ ions on the activity and hydrothermal stability. *Appl Catal B* 2017; **217**: 421–8.
78. Usui T, Liu Z and Ibe S *et al.* Improve the hydrothermal stability of Cu-SSZ-13 zeolite catalyst by loading a small amount of Ce. *ACS Catal* 2018; **8**: 9165–73.
79. Wang J, Peng Z and Qiao H *et al.* Cerium-stabilized Cu-SSZ-13 catalyst for the catalytic removal of NO_x by NH_3. *Ind Eng Chem Res* 2016; **55**: 1174–82.
80. Wang Y, Shi X and Shan Y *et al.* Hydrothermal stability enhancement of Al-Rich Cu-SSZ-13 for NH_3 selective catalytic reduction reaction by ion exchange with cerium and samarium. *Ind Eng Chem Res* 2020; **59**: 6416–23.
81. Zhao Z, Yu R and Shi C *et al.* Rare-earth ion exchanged Cu-SSZ-13 zeolite from organotemplate-free synthesis with enhanced hydrothermal stability in NH_3-SCR of NO_x. *Catal Sci Technol* 2019; **9**: 241–51.
82. Fan C, Chen Z and Pang L *et al.* Steam and alkali resistant Cu-SSZ-13 catalyst for the selective catalytic reduction of NO_x in diesel exhaust. *Chem Eng J* 2018; **334**: 344–54.
83. Luo JY, Yezerets A and Henry C *et al.* Hydrocarbon poisoning of Cu-Zeolite SCR catalysts. *SAE Tech Pap* 2021; 2012-01-1096.
84. Selleri T, Nova I and Tronconi E *et al.* The impact of light and heavy hydrocarbons on the NH_3-SCR activity of commercial Cu- and Fe-zeolite catalysts. *Catal Today* 2019; **320**: 100–11.
85. Ye Q, Wang L and Yang RT. Activity, propene poisoning resistance and hydrothermal stability of copper exchanged chabazite-like zeolite catalysts for SCR of NO with ammonia in comparison to Cu/ZSM-5. *Appl Catal A* 2012; **427–8**: 24–34.
86. Xie L, Liu F and Ren L *et al.* Excellent performance of one-pot synthesized Cu-SSZ-13 catalyst for the selective catalytic reduction of NO_x with NH_3. *Environ Sci Technol* 2014; **48**: 566–72.
87. Raj R, Harold MP and Balakotaiah V. Kinetic modeling of NO selective reduction with C_3H_6 over Cu-SSZ13 monolithic catalyst. *Chem Eng J* 2014; **254**: 452–62.
88. Zones SI. Conversion of faujasites to high-silica chabazite SSZ-13 in the presence of N,N,N-trimethyl-1-adamantammonium iodide. *J Chem Soc Faraday Trans* 1991; **22**: 3709–16.
89. Han J, Jin X and Song C *et al.* Rapid synthesis and NH_3-SCR activity of SSZ-13 zeolite via coal gangue. *Green Chem* 2020; **22**: 219–29.
90. Shan Y, Shi X and Du J *et al.* SSZ-13 synthesized by solvent-free method: a potential candidate for NH_3-SCR catalyst with high activity and hydrothermal stability. *Ind Eng Chem Res* 2019; **58**: 5397–403.
91. Xiong X, Yuan D and Wu Q *et al.* Efficient and rapid transformation of high silica CHA zeolite from FAU zeolite in the absence of water solvent. *J Mater Chem A* 2017; **5**: 9076–80.
92. Chen B, Xu R and Zhang R *et al.* Economical way to synthesize SSZ-13 with abundant ion-exchanged Cu^+ for an extraordinary performance in selective catalytic reduction (SCR) of NO_x by ammonia. *Environ Sci Technol* 2014; **48**: 13909–16.
93. Wang X, Zhang R and Wang H *et al.* Strategy on effective synthesis of SSZ-13 zeolite aiming at outstanding performances for NH_3-SCR process. *Catal Surv Asia* 2020; **24**: 143–55.
94. Ren L, Zhu L and Yang C *et al.* Designed copper-amine complex as an efficient template for one-pot synthesis of Cu-SSZ-13 zeolite with excellent activity for selective catalytic reduction of NO_x by NH_3. *Chem Commun* 2011; **47**: 9789–91.
95. Schmieg SJ, Oh SH and Kim CH *et al.* Thermal durability of Cu-CHA NH_3-SCR catalysts for diesel NO_x reduction. *Catal Today* 2012; **184**: 252–61.
96. Blakeman PG, Burkholder EM and Chen HY *et al.* The role of pore size on the thermal stability of zeolite supported Cu SCR catalysts. *Catal Today* 2014; **231**: 56–63.
97. Moliner M, Franch C and Palomares E *et al.* Cu-SSZ-39, an active and hydrothermally stable catalyst for the selective catalytic reduction of NO_x. *Chem Commun* 2012; **48**: 8264–6.
98. Shan Y, Shan W and Shi X *et al.* A comparative study of the activity and hydrothermal stability of Al-rich Cu-SSZ-39 and Cu-SSZ-13. *Appl Catal B* 2020; **264**: 118511–20.
99. Du J, Shi X and Shan Y *et al.* Effects of SO_2 on Cu-SSZ-39 catalyst for the selective catalytic reduction of NO_x with NH_3. *Catal Sci Technol* 2020; **10**: 1256–63.
100. Zhu N, Shan W and Shan Y *et al.* Effects of alkali and alkaline earth metals on Cu-SSZ-39 catalyst for the selective catalytic reduction of NO with NH_3. *Chem Eng J* 2020; **388**: 124250–60.
101. Sonoda T, Maruo T and Yamasaki Y *et al.* Synthesis of high-silica AEI zeolites with enhanced thermal stability by hydrothermal conversion of FAU zeolites, and their activity in the selective catalytic reduction of NO_x with NH_3. *J Mater Chem A* 2015; **3**: 857–65.
102. Martin N, Boruntea CR and Moliner M *et al.* Efficient synthesis of the Cu-SSZ-39 catalyst for DeNO$_x$ applications. *Chem Commun* 2015; **51**: 11030–3.

103. Xu H, Chen W and Wu Q *et al.* Transformation synthesis of aluminosilicate SSZ-39 zeolite from ZSM-5 and beta zeolite. *J Mater Chem A* 2019; **7**: 4420–5.
104. Ryu T, Ahn NH and Seo S *et al.* Fully copper-exchanged high-silica LTA zeolites as unrivaled hydrothermally stable NH_3-SCR catalysts. *Angew Chem Int Ed* 2017; **56**: 3256–60.
105. Ahn NH, Ryu T and Kang Y *et al.* The origin of an unexpected increase in NH_3-SCR activity of aged Cu-LTA catalysts. *ACS Catal* 2017; **7**: 6781–5.
106. Wang A, Arora P and Bernin D *et al.* Investigation of the robust hydrothermal stability of Cu/LTA for NH_3-SCR reaction. *Appl Catal B* 2019; **246**: 242–53.
107. Ryu T, Kim H and Hong SB. Nature of active sites in Cu-LTA NH_3-SCR catalysts: a comparative study with Cu-SSZ-13. *Appl Catal B* 2019; **245**: 513–21.
108. Wang A and Olsson L. Insight into the SO_2 poisoning mechanism for NO_x removal by NH_3-SCR over Cu/LTA and Cu/SSZ-13. *Chem Eng J* 2020; **395**: 125048–59.
109. Jo D, Ryu T and Park GT *et al.* Synthesis of high-silica LTA and UFI zeolites and NH_3-SCR performance of their copper-exchanged form. *ACS Catal* 2016; **6**: 2443–7.
110. Jo D, Park GT and Ryu T *et al.* Economical synthesis of high-silica LTA zeolites: a step forward in developing a new commercial NH_3-SCR catalyst. *Appl Catal B* 2019; **243**: 212–9.
111. Kim J, Cho SJ and Kim DH. Facile synthesis of KFI-type zeolite and its application to selective catalytic reduction of NO_x with NH_3. *ACS Catal* 2017; **7**: 6070–81.
112. Han S, Tang X and Wang L *et al.* Potassium-directed sustainable synthesis of new high silica small-pore zeolite with KFI structure (ZJM-7) as an efficient catalyst for NH_3-SCR reaction. *Appl Catal B* 2021; **281**: 119480–7.
113. Jo D, Lim JB and Ryu T *et al.* Unseeded hydroxide-mediated synthesis and CO_2 adsorption properties of an aluminosilicate zeolite with the RTH topology. *J Mater Chem A* 2015; **3**: 19322–9.
114. Shan Y, Shi X and Du J *et al.* Cu-exchanged RTH-type zeolites for NH_3-selective catalytic reduction of NO_x: Cu distribution and hydrothermal stability. *Catal Sci Technol* 2019; **9**: 106–15.
115. Xu H, Wu Q and Chu Y *et al.* Efficient synthesis of aluminosilicate RTH zeolite with good catalytic performances in NH_3-SCR and MTO reactions. *J Mater Chem A* 2018; **6**: 8705–11.
116. Martín N, Paris C and Vennestrøm PNR *et al.* Cage-based small-pore catalysts for NH_3-SCR prepared by combining bulky organic structure directing agents with modified zeolites as reagents. *Appl Catal B* 2017; **217**: 125–36.
117. Ke Q, Sun T and Cheng H *et al.* Accelerated construction of high-silica RHO and CHA zeolites via interzeolite transformation and their NH_3-SCR performances after copper exchange. *Ind Eng Chem Res* 2018; **57**: 16763–71.
118. International Zeolite Association Structure Commission. *Database of Zeolite Structures*. https://asia.iza-structure.org/IZA-SC/ftc_table.php (7 January 2021, date last accessed).